Role of channels in the O_2 permeability of murine red blood cells
I. Stopped-flow and hematological studies

Pan Zhao[1], Fraser J. Moss[1*], Rossana Occhipinti[1*], R. Ryan Geyer[1], Dale E Huffman[1], Howard J Meyerson[2], Walter F Boron[1, 3]

[1]Department of Physiology & Biophysics and [2]Department of Pathology
Case Western Reserve University School of Medicine
Cleveland, OH 44106
Medizinische Hochschule Hannover, Hannover, Germany
[3]Department of Medicine and Department of Biochemistry
Case Western Reserve University School of Medicine

*These authors made equal contributions to the work

Section: *Journal of Physiology*, Cell physiology

Running title: RBC O_2 permeability: Physiology

Keywords: Aquaporin 1, Rhesus (Rh) complex, genetic deletion, pCMBS (p-chloromercuribenzenesulfonate), DIDS (4,4'-diisothiocyanatostilbene-2,2'-disulfonate)

Correspondence and proofs:
Walter F Boron, MD, PhD
Department of Physiology and Biophysics
Case Western Reserve University
School of Medicine
10900 Euclid Avenue
Cleveland, OH 44106-4970
Phone: (216) 368 3400
Fax: (216) 368 5586
E-mail Walter.Boron@case.edu

Key Points

- Some hold that red-blood-cell (RBC) membranes have a finite O_2 permeability governed by O_2 solubility in membrane lipids; others, that the membranes offer no resistance whatsoever to O_2 diffusion.
- The present interdisciplinary study comprises three papers. This first paper describes stopped-flow absorbance spectroscopy in which we examine the rate constant of O_2 offloading from intact RBCs (k_{HbO_2}) from wild-type (WT) mice or those lacking AQP1 and/or RhAG, sometimes treated with p-chloromercuribenzenesulfonate (pCMBS) or 4,4'-diisothiocyanatostilbene-2,2'-disulfonate (DIDS).
- The second paper describes RBC morphometry and membrane proteomics. The third introduces a mathematical reaction-diffusion model that generates simulations that comport with physiological data.
- This first paper shows that pCMBS or DIDS treatments, or deletion of AQP1 and/or RhAG, or combinations thereof, reduce k_{HbO_2}.
- We conclude that WT RBC membranes offer substantial resistance to O_2 diffusion. AQP1 (~22%), Rh (~36%), and an unknown pCMBS-sensitive protein (~35%) account for ~91% of membrane O_2 permeability.

Abstract

Many have believed that oxygen (O_2) crosses red blood cell (RBC) membranes by dissolving in lipids that offer a finite resistance to diffusion or, alternatively, no resistance at all. However, analyses of hemoglobin (Hb) absorbance spectra during O_2 off-loading from mouse RBCs indicate that RBC membranes do indeed offer resistance to O_2 diffusion, and that the resistance would be far higher if not for the presence of O_2-permeable channels. Two agents—both excluded from the RBC interior—markedly slow O_2 off-loading: p-chloromercuribenzenesulfonate (pCMBS) reduces membrane O_2 permeability (P_{M,O_2} by ~82%, and 4,4'-diisothiocyanatostilbene-2,2'-disulfonate (DIDS) by ~56%. Because neither likely produces these effects via membrane lipids, we examined RBCs from mice genetically deficient in aquaporin-1 (AQP1), the Rh complex (Rh_{Cx} = Rhesus blood group-associated A glycoprotein, RhAG + Rhesus blood group D antigen, RhD), or both. The double knockout (dKO) reduces P_{M,O_2} by ~55%, and pCMBS+dKO, by ~91%. Proteomic analyses of RBC membranes, flow cytometry, hematology, and mathematical simulations rule out meaningful contributions from other membrane proteins, RBC geometry, or extracellular unconvected fluid (EUF). Our work represents a paradigm shift for O_2 physiology by identifying the first two animal O_2 channels, and points to the existence of at least a third, all of which could be subject to physiological regulation and pharmacological intervention.

Introduction

Central to human life is the inhalation of oxygen (O_2), its diffusion across the alveolar wall to pulmonary capillary blood plasma, O_2 diffusion inward across the red blood cell (RBC) membrane and transfer to hemoglobin (Hb; $Hb + O_2 \rightarrow HbO_2$),[1] distribution of RBCs by blood flow throughout the body, O_2 offloading from Hb, and finally O_2 diffusion outward across the RBC membrane and other barriers to support oxidative metabolism. Critical to understanding this journey of O_2 from air to mitochondria is the diffusion of O_2 across various membranes, particularly that of the RBC.

Since the early 1800s, the mechanisms by which gases move across natural and artificial barriers have been the focus of numerous investigations (Graham, 1829, 1833; Mitchell, 1830, 1831*a*, 1831*b*, 1833; Fick, 1855; Overton, 1895; reviewed by Stannett, 1978). For example, Mitchell was the first to recognize that the "facility of transmission" (i.e., permeation) of gases through (primarily synthetic) membranes depends on their "power of infiltration" (i.e., solubility) in the organic molecular barrier (Mitchell, 1831*a*, 1831*b*). This was the first statement of "solubility theory" (see Stannett, 1978). Subsequently, Graham, who gave us Graham's law, hypothesized that gas permeation across barriers depends on the ability of the gas not only to dissolve in the barrier but also to diffuse through it—the first statement of solubility-diffusion theory. In 1879, Wroblewski combined Mitchell's and Graham's observations with Henry's law of gas solubility in liquids (Henry, 1803) and Fick's law of diffusion to produce our current, simplified mathematical description of the solubility-diffusion theory (Wroblewski, 1879; for

---

[1] We use HbO_2 to represent the generic oxygenated hemoglobin (i.e., oxyhemoglobin). Of course, under physiological conditions at sea level, the Hb tetramer enters the mammalian lung with 3 O_2 bound on average, $Hb(O_2)_3$, and exits with four bound on average $Hb(O_2)_4$.

reviews, see Stannett, 1978; Cooper *et al.*, 2015; Michenkova *et al.*, 2021). In the late 1890s, Overton—whose aim was to determine whether biological membranes have a lipid component—showed that membrane permeability is proportional to the lipophilicity (i.e., the lipid-water partition coefficient) of the permeating molecule (Overton, 1895, 1899). Although Overton's experiments were far more elegant than those of Mitchell, his conclusion was a restatement of Mitchell's solubility theory. Over the years, biologists—like Overton, apparently unaware of the work of Mitchell—began to refer to Overton's observations as "Overton's rule", even though Mitchell's solubility theory predated Overton by more than 60 years, and the "rule" altogether ignores Graham's more inclusive solubility-diffusion theory that predated Overton by 30 years.

Thus, in the early 20th century, many biologists believed that the resistance that membranes offer to the diffusion of gases depends only on the solubility of the gas in the lipid phase of the membrane. Later work on the diffusion of carbon dioxide (CO_2) through artificial lipid membranes by Blank & Roughton, (1960), Gutknecht *et al.*, (1977), and Simon & Gutknecht, (1980) showed that the diffusion component of solubility-diffusion theory is quantitatively far more important than the solubility component (see review by Boron, 2010). Nevertheless, the concept that gases cross membranes merely by dissolving in the lipid phase of the membrane—Overton's rule—became dogma, at least for most physiologists.

Interestingly, with a smaller group of 20th-century physiologists—influenced by the pioneering work of Krogh on O_2 offloading from RBCs and delivery to the tissues (Krogh, 1919)—a very different dogma evolved. Krogh's mathematical analysis of the "Krogh cylinder" required the implicit, simplifying assumption (see Kreuzer, 1982) that the various cell membranes, including the RBC membrane, offer no resistance to O_2 diffusion. Although some argued otherwise (Hartridge & Roughton, 1927; Forster, 1964), Krogh's implicit assumption became engrained in the literature. Roughton, (1932), and many came to believe that O_2 crosses RBC membranes simply by dissolving in lipids that offer no resistance whatsoever to diffusion.

Calling the above prevailing views into question were two discoveries, namely, the identification of: (1) membranes with no detectable CO_2 permeability (Waisbren *et al.*, 1994), specifically the apical (i.e., lumen-side membranes) of chief and parietal cells of gastric-glands; and (2) a membrane protein (i.e., aquaporin-1, AQP1; Preston & Agre, (1991); Preston *et al.*, (1992)) with an additional role as a CO_2 channel (Nakhoul *et al.*, 1998; Cooper & Boron, 1998). The reagent p-chloromercuribenzenesulfonate (pCMBS), which reacts with the –SH of Cys-189 in the extracellular vestibule of the AQP1 monomeric pore, not only inhibits H_2O movement through AQP1 (Preston *et al.*, 1993), but also blocks a component of CO_2 traffic through AQP1 (Cooper & Boron, 1998). Moreover, various AQPs exhibit CO_2 vs. NH_3 selectivity (Musa-Aziz *et al.*, 2009; Geyer *et al.*, 2013). Other work showed that rhesus (Rh) proteins also can conduct CO_2 (Endeward *et al.*, 2008). These observations revealed that gas transport across membranes must involve more than that predicted by solubility-diffusion theory: the solvation into the lipid bilayer, diffusion through the bilayer, and the desolvation at the opposite side of the bilayer. Work on human RBCs genetically deficient in AQP1 (Endeward *et al.*, 2006) or the Rhesus blood group-associated A glycoprotein RhAG (Endeward *et al.*, 2008) established that AQP1 and the Rh complex (Rh_{Cx}= RhAG + RhD) together account for >90% of CO_2 permeability of RBCs. Moreover, that work established that 4,4'-diisothiocyanatostilbene-2,2'-disulfonate (DIDS), which binds to and can react with the $–NH_3^+/NH_2$ moiety of Lys residues, blocks a component of CO_2 traffic through both AQP1 and Rh_{Cx}. Although neither pCMBS nor DIDS is specific, both are valuable tools because (as we will see in the present paper) they do not enter RBCs, and they have minimal presence in the lipid phase of the plasma membrane (Vansteveninck *et al.*, 1965; Rothstein *et al.*, 1973; Cabantchik & Rothstein, 1974). Thus, we hypothesized that, like CO_2, O_2 crosses RBC membranes mainly via channels, and that pCMBS or DIDS would block these hypothetical O_2 channels.

The present study comprises three tightly interwoven papers that aim to determine the extent to which AQP1, Rh_{Cx}, and potentially other RBC membrane proteins contribute to the O_2 permeability of the RBC membrane (P_{M,O_2}).

In this first (the present) paper, we use stopped-flow (SF) absorbance spectroscopy to determine the rate constant for Hb deoxygenation (k_{HbO2}) as we mix oxygenated murine RBCs with a solution containing the O_2 scavenger sodium dithionite (NDT). This first paper also examines the channel inhibitors pCMBS and DIDS, and also RBCs from mice genetically deficient in AQP1, RhAG, or both (i.e., double knockouts, dKO). Recognizing that differences in k_{HbO2} associated with drugs or knockouts (KOs) could reflect changes in parameters other than P_{M,O_2}, we also examine the kinetics of the reaction $HbO_2 \rightarrow Hb + O_2$ as well as mean corpuscular volume (MCV) and mean corpuscular hemoglobin concentration (MCHC) and other hematological parameters. This first paper also serves as the overall summary of the three-paper project by briefly summarizing, in context, key elements of the other two papers, and providing references to specific locations in those papers.

The second paper (i.e., paper #2; Moss *et al.*, 2025) complements the first by examining RBC morphology at a microscopic scale, including measurements of RBC major diameter ($Ø_{Major}$; i.e., maximum dimension) using imaging flow cytometry (IFC). These data, together with MCV data from the present paper, allow us to estimate RBC thickness. These data also identify cells that are not biconcave disks. In addition, this paper includes a proteomic analysis that confirms that the RBC membranes of genetically deficient mice lack only the intended proteins among the 100 proteins with the greatest inferred abundance.

In the third paper (i.e., paper #3; Occhipinti *et al.*, (2025)) we report a novel mathematical reaction-diffusion model, based on first principles, in which we treat the RBC as a sphere with a diameter that reflects the computed RBC thickness. Together with physical constants, parameter values from the literature, and data from the first two papers, this model generates simulations that

are in good agreement with the physiological data, allowing us to extract P_{M,O_2} values from k_{HbO2} and other wet-lab data.

The overall conclusion of the three papers is that, contrary to the implicit assumption of Krogh, RBC membranes of wild-type (WT) mice offer considerable resistance to O_2 diffusion, with a computed permeability ~200 times greater than an equivalent layer of water. AQP1 (~22%) and Rh_{Cx} (~36%) account for ~55% of the usual P_{M,O_2}. Moreover, at least one other pCMBS-sensitive protein is responsible for an additional ~35%, so that that total protein-mediated component of P_{M,O_2} is at least ~90%. Thus, this work changes the way we think of RBC O_2 handling, and raises the possibility of modulating P_{M,O_2} by manipulating membrane proteins.

Methods

Ethical approval and animal procedures

All animal procedures were reviewed and approved by the Institutional Animal Care and Use Committee (IACUC) at Case Western Reserve University (CWRU).

Mice

We originally obtained as *Aqp1*+/– mice—with a targeted disruption (replacement of the last 24 bp of exon 1 and 1.3 kb of intron 1 by the 1.8-kb PolII-neo selectable marker) of the *Aqp1* gene (Ma *et al.*, 1998)—on a "C57BL/6" background (Kelmenson, 2016), as a generous gift of Alan Verkman. The *Aqp1*+/+ mice obtained from the initial crosses were backcrossed for >20 generations by our laboratory to define our lab-standard WT strain, C57BL/6_{Case}.

We backcrossed *Aqp1*+/– mice into our WT mice for >18 generations, and confirmed genotypes (see Genotyping). We backcrossed *Rhag*+/– mice (provided by Jean-Pierre Cartron as *Rhag*+/– mice on a C57/BL6 background), with a targeted disruption between exon 1 and 2 of the *Rhag* gene (Goossens *et al.*, 2010), into our WT mice for at least 7 generations, and confirmed genotypes (see Genotyping). From *Aqp1*–/– and *Rhag*–/– mice, we generated dKO (i.e., *Aqp1*–/– *Rhag*–/–) mice, and confirmed genotypes as described below (see Genotyping).

We contracted with TransnetYX, Inc. (Cordova, TN) to perform Genetic Background analysis on our four mouse strains, all on a C57BL/6_{Case} background. TransnetYX examined all ~10,000 single-nucleotide polymorphisms (SNPs) in their catalog, SNPs from >200 strains of mice. These included 156 SNPs specific for C57BL/6J (from Jackson Laboratory), 31 SNPs for C57BL/6N (from the National Institutes of Health), and 21 SNPs for C57BL/6Group (characteristic of other C57BL/6 strains). Table 1 summarizes the results of this analysis, which shows that our C57BL/6_{Case} mice are on average ~19.6% C57BL/6J, ~20.6% C57BL/6N, ~25.6% C57BL/6Group, for a total BL/6 character of ~65.8%.

Mice were allowed access to food and water ad libitum. In experiments, we used mice of both sexes (8 to 19 weeks old). Not shown are data indicating that no changes in kinetic or hematological parameters occur up to 6 months of age for all genotypes. All animal procedures were reviewed and approved by the Institutional Animal Care and Use Committee (IACUC) at Case Western Reserve University.

Genotyping

WT vs. *Aqp1*+/– vs. *Aqp1*–/– are genotyped by real-time PCR (performed by TransnetYX, Inc., Cordova, TN). For detecting the *Aqp1*– allele, the forward primer is 5′-CAC CTC GGT AGC AAC TCG AA-3′, the reporter primer 1 is 5′-CTC CTC GAA GGA ATT C-3′, and the reverse primer is 5′-GGG CTC GAG ATC CAC TAG ACT-3′. For detecting WT, the forward primer is 5′-CTT AGG CTT AGG GTG TCT GTA GGA-3′, the reporter primer 1 is 5′-CTG GCT CCA TTT GCC-3′, and the reverse primer is 5′-CTT CAT CCT TCT CTC TGT TCT TCA GT-3′.

WT vs. *Rhag*+/– vs. *Rhag*–/– mice are genotyped by real-time PCR (performed by TransnetYX, Inc.) to determine the presence of a *Rhag*–allele. For detecting the KO allele, the forward primer is 5′-TGC TGC TAT GAC CAT TGG AA-3′, and the reverse primer is 5′-ATT GCA TCG CAT TGT CTG AG-3′. The KO PCR results 196-bp band.

If we detect a KO allele in a mouse, we must differentiate between a *Rhag*+/– and *Rhag*–/– mouse by attempting to detect the WT allele. We perform this assay in house because the PCR product is long (~8 kb). We prepare highly purified genomic DNA from tail tissue using the DNeasy Blood and Tissue Kit (Qiagen, Germantown, MD), and perform *Rhag*-WT genotyping. Primer "*Rhag*-WT 3F" (5′-TGA AAT GTT TAA TGC TCA TCG ACC AC-3′) is designed to anneal to the end of Intron 1–2 of *Rhag*, and Primer "*Rhag*-WT 3R" (5′-GAG TGA CTT CA CCT TCT TAT CTT CTA AG-3′), to the middle of intron 6–7. The *Rhag*-WT PCR product is ~8 kb, as noted above, using the Qiagen Long Range (LR) PCR Kit. Presence of the WT-PCR product

confirms a *Rhag*+/– genotype for any mouse reported to be positive for *Rhag*–/– by TransnetYX. Absence of a WT-PCR product confirms the *Rhag*–/– genotype.

Physiological solutions

Table 2 shows the compositions of all solutions used in this study. We made pH measurements—either at room temperature (RT) or at 10°C—using a portable pH meter (model A121 Orion Star, Thermo Fischer Scientific (TFS), Waltham, MA) fitted with a pH electrode (Ross Sure-Flow combination pH Electrode, TFS). Beakers containing pH calibration buffers (pH at 6, 8 and 10; TFS), physiological solutions to be titrated, and the pH electrode in its storage solution (Beckman Coulter, Inc. Brea, CA) were equilibrated at either RT or 10°C, as appropriate. For work at 10°C, we used a refrigerated, constant-temperature, shaker water bath (model RWB 3220, TFS) and submersible Telesystem magnetic stirrers (TFS). We adjusted pH with NaOH (5 M) or HCl (5 M). Osmolality was measured using a vapor pressure osmometer (Vapro 5520; Wescor, Inc., Logan, UT) and, as necessary, adjusted upward by addition of NaCl.

Inhibitors

Stock solutions of 2 mM pCMBS (catalog no. C367750; Toronto Research Chemicals, Toronto, ON, Canada) and 2 mM DIDS (catalog no. 1226913; Invitrogen, Eugene, OR) were freshly prepared by dissolving the agents directly into either our "Oxygenated solution" or solution "$\mathcal{A}$" (see Table 2), taking care to shield the solutions from light.

Preparation of RBCs

Collection of blood from mice. We collected fresh blood from WT or KO mice for seven assays: (1) SF, (2) still microphotography, (3) microvideography, (4) flow cytometry, (5) automated hematology, (6) blood smears, and (7) proteomics/mass spectrometry. Early on (only for SF studies), we used the cardiac-puncture method (Parasuraman *et al.*, 2010). Later (for the remaining SF and all other studies), so that we could return to the same mouse for more than one

sample of blood, we used the submandibular-bleed method (Golde *et al.*, 2005). For cardiac puncture, we used a 1-ml syringe (Becton, Dickinson and Co., Franklin Lakes, New Jersey) and attached 23-gauge PrecisionGlide needle (Becton, Dickinson and Co). For bleeds of the submandibular vein, we used a 3-, 4-, or 5-mm point-length sterile animal lancet (MEDIpoint, Inc., Mineola, NY), and took blood samples (~200 μl) from the same mouse no sooner than 72 h from a previous blood sample, and on the contralateral side.

Processing of RBCs for assays 1–4. For the first four assays (SF, still microphotography, microvideography, flow cytometry), we collected the blood into 1.7-ml microcentrifuge tubes (Laboratory Products Sales Inc. Rochester, N.Y.) that we had previously rinsed with 0.1% sodium heparin (H4784, Sigma-Aldrich, St. Louis, MO), and then centrifuged in a Microfuge 16 Microcentrifuge (Beckman Coulter, Inc.) at 600 × g for 10 min. We aspirated and discarded the resulting supernatant and buffy coat. To remove residual extracellular Hb, we resuspended the pelleted RBCs in our oxygenated solution (see Table 2) to a hematocrit (Hct) of 5% to 10%, centrifuged at 600 × g for 5 min. After 4 such washes, we resuspended RBCs in our oxygenated solution to a final Hct of 25% to 30%, and maintained on ice (for that day) for experiments. At this point, we continued with the processing of RBCs for SF studies (the present paper; see below [2]) or for the three studies in paper #2, namely, still microphotography, microvideography, or flow-cytometry.[3]

---

[2] See Methods>Preparation of RBCs>Processing of RBCs for stopped-flow studies. The ">" symbol separates heading levels. It is understood that the reference is to a location in the present paper unless "See" is followed by "Paper #2" or "Paper #3".

[3] See Paper #2>Methods>Preparation of RBCs>First four assays

Processing of RBCs for automated hematology. For automated hematological studies (see below[4]), we collected whole blood into 20-µl plastic Boule MPA Micro pipettes (EDTA-K2, Boule Medical AB, Stockholm, Sweden).

Processing of RBCs for blood smears. For blood smears,[5] we collected whole blood into 2-ml K2E K2EDTA VACUETTE® tubes (Grelner Bio-One North America Inc, Monroe, NC).

Processing of RBCs for proteomics. For proteomic analysis[6], we collected whole blood into 1.7-ml heparinized microcentrifuge tubes (see above[7]).

Processing of RBCs for stopped-flow studies. For SF studies, after collection of the blood (see above[8]), we computed [Hb] in a suspension of intact RBCs from the Hb absorbance measured on a UV/Vis spectrophotometer (model 730 Life Science, Beckman Coulter, Inc.), using an equation described previously (Zhao *et al.*, 2017).

As necessary, we produced an RBC lysate by osmotic lysis of 20 µl of freshly prepared, packed mouse RBCs in a 1:8~1:10 dilution of Milli-Q H_2O (Milli-Q® Integral Water Purification System, EMD Millipore Corporation, Billerica, MA), followed by centrifugation at 15000 × g for

---

[4] See Methods>Automated hematological analyses (workflow #7-9)

[5] See Paper #2>Methods>Blood smears

[6] See Paper #2>Methods>Proteomic analysis

[7] See Methods>Preparation of RBCs>Processing of RBCs for assays 1–4

[8] See Methods>Preparation of RBCs>Collection of blood from mice

5 min in a Microfuge 16 Microcentrifuge, at RT. We transferred the supernatant to a clean 1.7-ml microcentrifuge tube for a spectroscopic determination of free [Hb], as described previously (Zhao *et al.*, 2017).

For all stopped-flow experiments—on intact RBCs or lysates or mixtures thereof—we dilute the material to a [Hb] of 5 μM before introduction into the SF device. After mixing in the SF reaction cell, [Hb] falls to a final values of 2.5 μM. In the case of deoxygenation assays (e.g., in Results, see Figure 3 and Figure 4), the diluent was the oxygenated solution (see Table 2). In the case of carbonic-anhydrase assays (e.g., in Results, see summary in Figure 6; see Zhao *et al.*, 2017), the diluent was solution "$\mathcal{A}$" (see Table 2), which is also oxygenated.

Use of inhibitors in stopped-flow studies. In all inhibitor studies, except those in which we studied short-term exposures to DIDS (introduced next), we pre-incubated samples (either ostensibly intact RBCs or a hemolysate) with the drug before introduction into the SF device:

(1) pCMBS (1 mM): 15-min preincubation. In Results, for

(a) ostensibly intact RBCs, see Figure 3*C–D.* and filled bars in Figure 3*E–F*;

(b) hemolysate, see open bars in Figure 3*F*.

(2) DIDS (200 μM): 60-min preincubation. In Results, for

(a) ostensibly intact RBCs, see Figure 4*C–D* and filled bars in Figure 4*E–F*;

(b) hemolysate, see open bars in Figure 4*F* and filled gray-blue bars in Figure 8*A*).

The next step, for both drugs, was to dilute the material in our oxygenated solution (see Table 2) to achieve a [Hb] of 5 μM plus either 1 mM pCMBS or 200 μM DIDS, added from a

stock solution (see "Inhibitors", above[9]). Finally, we performed stopped-flow studies by mixing the aforementioned oxygenated solution with the deoxygenated solution (see Table 2) to obtain k_{HbO_2}.

In a few studies, we assessed the effect of millisecond-to-second DIDS exposures on Hb absorbance spectra of hemolysates (e.g., in Results, see Figure 8*B*, gray-blue open bars). Here, we did not preincubated the hemolysate in DIDS. Rather, we placed (1) the lysate in the oxygenated solution and (2) the DIDS in the deoxygenated solution (see Table 2). Thus, the DIDS did not contact the Hb in the lysate until reaching the SF reaction cell as we determined k_{HbO_2}.

Stopped-flow absorbance spectroscopy (workflow #1)

The flow chart in Figure 1 describes the series of steps—starting with the time course of RBC absorbance spectra (workflow: step #1) introduced in this section—we made a series of corrections to arrive at refined estimates for k_{HbO_2} and the associated P_{M,O_2}.

We use an SX-20 stopped-flow apparatus (Applied Photophysics, Leatherhead, UK) in absorbance spectroscopy mode to determine the rate constant of hemoglobin deoxygenation. We load RBCs or RBC/ hemolysate mixtures or pure hemolysate ([Hb] = 5 μM, Hct ≅ 0.4%), suspended in our oxygenated solution (see Table 2), into one syringe of the SF apparatus. We load the deoxygenated solution containing the O_2 scavenger NDT (50 mM; SIGMA-ALDRICH, Co, St, Louis, MO) into the other syringe. We record absorbance (*A*) in a 20-μl SF reaction cell (2-mm path length) at 10°C, over the portion of the Hb spectrum with highest Signal/Noise (wavelength [λ]: 410–450 nm, at 5 nm intervals), sampling at 10-ms intervals for 4000 ms. For each new set of loaded samples, we begin by performing ≥6 "shots" to ensure that the new solutions are loaded

[9] See Methods>Inhibitors

into the SF reaction cell, and then sequentially acquire A_λ vs. time during 9 separate shots at λ = 410, 415 … 450 nm—this constitutes one data set. We compile such data set into 3-D graphs (e.g., in Results, see A_λ vs. λ vs. time plots in Figure 3*A–B* and Figure 4*A–B*). We obtain at least 1 such data set (see criteria in next section)—but typically 2 to 4—for each set of experimental conditions, and then average these k_{HbO_2} values to obtain the "raw" k_{HbO_2} value used in further analyses.

The above sequence is step #1 in Figure 1.

Calculation of time course of HbO_2 desaturation (workflow #2)

The time course of the decay $HbO_2 \rightarrow Hb + O_2$ does not follow a perfect exponential function—nor should it according to our mathematical modeling (see paper #3). We therefore developed an unbiased approach[10] for computing the quasi-rate constant k_{HbO_2}, based on the time (t_{37}) required for O_2 saturation of Hb (HbSat) to fall to 1/e of its initial value. We proceed in the following sequence:

Preprocess data. We eliminate noisy absorbance data—which we standardize as the first 9 points (0.010 – 0.090 s)—and translate the time axis so that raw data at absolute times 0.100 – 4.000 s now covers the relative time range 0.000 – 3.900 s. We also eliminate data at 3 wavelengths (420, 445, 450 nm) that are close to isosbestic points because, at these wavelengths, absorbance values do not change consistently during an experiment. The result is a data set describing A_λ vs. relative time (from 0.000 to 3.900 s) at each of 6 wavelengths (λ = 410, 415, 425,

[10] The "Pro-KIV" software supplied by Applied Photophysics assumes that the absorbances at all wavelengths decay as a perfect exponential, and fits them all simultaneously, producing a single time constant/rate. Because this approach could introduce a bias into the analysis, we developed the method described here. Nevertheless, the two approaches produce numerical results that differ only slightly, and do not affect the conclusions that we draw.

430, 435, and 440 nm). We accept a data set only if each of the 6 records of A_λ vs. time approaches an asymptote.

Obtain data parameters. For each of 6 plots of A_λ vs. time, obtain the minimum ($A_{\lambda,\mathrm{min}}$) and maximum values ($A_{\lambda,\mathrm{max}}$), as well as the difference $\Delta A_\lambda = A_{\lambda,\mathrm{max}} - A_{\lambda,\mathrm{min}}$ (i.e,. magnitude of the absorbance change). The 6 values of ΔA_λ become weighting factors, applied two paragraphs below.

Normalize. Perform a vertical flip of plots of A_λ vs. time that were originally concave downwards (these are λ = 425, 430, 435, 440 nm), so that all plots are now concave upwards. Vertically translate each plot of A_λ vs. time so that the minimum value is zero. Normalize each plot of A_λ vs. time so that $A_{\lambda,\mathrm{max}}$ is now unity.

Apply weighting factors. Normalize the 6 weighting factors (i.e., ΔA_λ) so that they sum to unity. Multiply each plot of A_λ vs. time by its weighting factor. At each time point, sum the 6 weighted A_λ values to obtain relative HbSat. The resulting plot of relative HbSat thus falls from unity to zero as relative time increases from 0.000 s to 3.900 s. Note that—because the RBCs or Hb are equilibrated in room air before being loaded into the SF device—the actual HbSat falls from a value of ~98% when the RBCs first enter the SF reaction cell at absolute time 0.000 s, and has already fallen to some extent by the time of our first accepted sample at absolute time 0.100 s, and then continues to fall to zero during the remaining 3.900 s of the "shot."

The above sequence is step #2 in Figure 1.

In Results, Figure 3*C*, Figure 4*C*, and Figure 5*A–C* show examples of the final product of such analyses, that is, plots of HbSat vs. time.

Calculation of "raw"-k_{HbO2} (workflow #3)

Examining the plot of relative HbSat vs. relative time data (see above[11]), we estimate t_{37}. We then identify the 5 relative HbSat points to the left[12] and the 5 points to the right of the estimated t_{37}, and fit the 11 points with a polynomial of degree 2, and solve the best-fit polynomial for the actual relative t_{37}, and compute the "raw" k_{HbO_2} as $1/t_{37}$.

The above sequence is step #3 in Figure 1.

Quantitation of hemolysis in SF reaction cell (workflow #4)

We have developed a novel assay (not depicted here; see Zhao *et al.*, 2017), based on the activity of carbonic anhydrase (CA), for determining the degree of RBC hemolysis in the SF reaction cell in a time domain similar to that of our O_2-efflux experiments (e.g., in Results, see Figure 3*A–B*). We use the SF apparatus to mix solutions A and B (see Table 2) in the SF reaction cell, and create an out-of-equilibrium (OOE) CO_2/HCO_3^-/pH state, chosen to be too low for equilibrium. The OOE solution then re-equilibrates according to the reaction $HCO_3^- + H^+ \rightarrow CO_2 + H_2O$ (i.e., raising pH), catalyzed by CA released from hemolyzed RBCs.

Solution A contains HEPES/pH 7.03 + RBCs or hemolysate. Solution B contains ~1% CO_2/44 mM HCO_3^-/pH 8.41 + the fluorescent pH-sensitive dye pyranine (H348, Invitrogen), which reports extracellular pH (pH_o). We excite the dye at 460 nm or 415 nm, while monitoring total fluorescence emission using a 488-nm long-pass filter. Immediately upon mixing of A and B, the solution in the SF reaction cell (10°C) has the composition ~0.5% CO_2/22 HCO_3^-/pH ~7.25, which

---

[11] See Methods>Calculation of time course of HbO_2 desaturation>Apply weighting factors

[12] In some cases, HbSat fell so rapidly that we were forced to use < 5 points to the left.

is out of equilibrium. The pH_o rises exponentially (rate constant, $k_{\Delta pH}$, computed as described previously (Zhao *et al.*, 2017)) to ~7.50.

We calculate the actual percent hemolysis (*Act%H*) of ostensibly 100% intact RBCs (i.e., apparent percent hemolysis, *App%H*, is 0%) during a SF experiment, as described previously (Zhao *et al.*, 2017), using a procedure that requires three rate constants: k_{uncat}, $k_{RBC,Lysate}$, and $k_{RBC,OstInt}$. (1) k_{uncat} is the uncatalyzed $k_{\Delta pH}$ (without CA). (2) $k_{RBC,Lysate}$ is $k_{\Delta pH}$ in the presence of fully lysed RBCs. Finally, (3) $k_{RBC,OstInt}$ is $k_{\Delta pH}$ in the presence of ostensibly 100% intact RBCs. From these, we compute $k_{cat,min} = k_{RBC,OstInt} - k_{uncat}$ and $k_{cat,max} = k_{RBC,Lysate} - k_{uncat}$. Finally:

$$Act\%H_{\mathrm{App}\%H=0\%} = \frac{k_{\mathrm{cat,min}}}{k_{\mathrm{cat,max}}} .$$

The above equation yields the actual percent hemolysis at a time when the apparent % hemolysis is 0%.

The above sequence is step #4 in Figure 1.

Accommodation for hemolysis (workflow #5)

Control and pCMBS-treated RBCs. Because Hb released into free solution deoxygenates faster than Hb inside RBCs, we correct "raw"-k_{HbO_2} values (step #3 in Figure 1), based on actual % hemolysis values (step #4 in Figure 1). For each mouse, we generate simulated hemolysis samples for apparent hemolysis levels of 0% (i.e., ostensibly 100% intact RBCs), 2.5%, 5%, 10% and 25% by mixing ostensibly 100% intact RBCs (at relative levels of 100%, 97.5%, 95%, 90%, and 75%) with hemolysate (at relative levels of 0%, 2.5%, 5%, 10%, and 25%)—

keeping total [Hb] constant at 5 μM. We determine "raw"-k_{HbO_2} (see above[13]) for each of these simulated hemolysis samples, and—using an algebraic scaling and translation of the x-axis—convert a plot of k_{HbO_2} vs. *App%H* (e.g., in Results, see blue axes in Figure 7*B* and *D*) to a plot of k_{HbO_2} vs. *Act%H* (see green axes). Extrapolating k_{HbO_2} back to 0% actual hemolysis yields an estimate of the actual k_{HbO_2} of 1 mouse. We used this approach for all experiments for RBCs treated with pCMBS or no drug.

The above sequence—for RBCs exposed to no drug or to pCMBS—is step #5 in Figure 1.

DIDS-treated RBCs. For RBCs treated with DIDS, we modified the above[14] approach because DIDS decreases the k_{HbO_2} of free Hb, so that the actual slope of the k_{HbO_2} vs. *Act%H* regression line ($Slope_{DIDS,Act}$) is less than the control value ($Slope_{Ctrl,Act}$). Two factors are at work. (1) During the 1-h pretreatment of RBCs with DIDS, the drug produces a substantial reduction in k_{HbO_2} (in Results, see Figure 8*A*), although this affects only a minute fraction of RBCs that have hemolyzed before entry into the SF device (see Zhao *et al.*, 2017). (2) During the actual SF experiment, DIDS produces a small reduction in k_{HbO_2} (in Results, see Figure 8*B*) for a larger fraction of Hb newly released in the SF reaction cell over a millisecond/second time frame. For Figure 8*A* and *B*, we obtained Hb and exposed it to DIDS as described in the figure legends.

In a DIDS experiment, the actual slope of the regression line becomes:

---

[13] See Methods>Calculation of "raw"-k_{HbO_2}

[14] See Methods>Accommodation for hemolysis (workflow #5)>Control and pCMBS-treated RBCs

$$Slope_{\mathrm{DIDS,Act}} = Slope_{\mathrm{Ctrl,Act}} \left[\underbrace{\underbrace{\frac{k_{\mathrm{HbO_2DIDS,1\text{-}h}}}{k_{\mathrm{HbO_2Ctrl}}}}_{\substack{\text{\% remaining after}\\ \text{1-h DIDS}}} \cdot \underbrace{\frac{\%H_{\mathrm{RBCs,Washed}}}{\%H_{\mathrm{RBCs,RxCell}}}}_{\substack{\text{\% [Hb]}_{\mathrm{o}}\text{ exposed}\\ \text{to DIDS} \times \text{1 h}}}}_{\substack{\text{\% } k_{\mathrm{HbO_2}} \text{ that remains for the free Hb exposed}\\ \text{to DIDS for 1h in tube before SF}}} + \underbrace{\underbrace{\frac{k_{\mathrm{HbO_2DIDS,ms/s}}}{k_{\mathrm{HbO_2Ctrl}}}}_{\substack{\text{\% remaining after}\\ \text{ms/s DIDS}}} \cdot \underbrace{\frac{\%H_{\mathrm{RBCs,RxCell}} - \%H_{\mathrm{RBCs,Washed}}}{\%H_{\mathrm{RBCs,RxCell}}}}_{\substack{\text{\% [Hb]}_{\mathrm{o}}\text{ exposed}\\ \text{to DIDS} \times \text{ms/s}}}}_{\substack{\text{\% } k_{\mathrm{HbO_2}} \text{ that remains for the free Hb exposed}\\ \text{to DIDS for ms/s in SF reaction cell}}} \right]$$

(1)

Thus, knowing the $k_{\mathrm{HbO_2}}$ measured in ostensibly 100% intact RBCs ($k_{\mathrm{HbO_2DIDS,OstInt}}$), we can estimate the actual $k_{\mathrm{HbO_2}}$ for DIDS-treated RBCs as:

$$k_{\mathrm{HbO_2DIDS,Act}} = k_{\mathrm{HbO_2DIDS,OstInt}} - Slope_{\mathrm{DIDS,Act}} \cdot \left(Act\%H \right).$$

The above sequence—whether in the absence or presence of DIDS—is step #5 in Figure 1.

Measurement of major cell diameter (workflow #6)

As described in paper #2[15], we use imaging flow cytometry to measure the major diameter ($Ø_{\mathrm{Major}}$) of cells shaped as biconcave disks (BCDs) or non-biconcave disks (nBCDs). This is step #6 in Figure 1.

Automated hematological analyses (workflow #7– #9)

Assays on normal whole blood. We collect fresh whole blood into special pipettes (see above[16]), which we insert into a Heska HemaTrue® Veterinary Hematology Analyzer (Heska

[15] See Paper #2>Methods>Flow cytometry>Imaging flow cytometry

[16] See Methods>Preparation of RBCs>Processing of RBCs for automated hematology

corporation, Loveland, CO) according to the manufacturer's protocol. The HemaTrue® analysis yields a wide variety of parameters (introduced below in Table 4), including those related to white and red blood cells and platelets; Hct; hemoglobin; MCH (step #7 in the flowchart) and MCV (step #8 in the flowchart, Figure 1).

Use of inhibitors in automated hematological studies. After collecting fresh whole blood from WT or dKO mice, we processed the cells as in "first four assays" (see above[17]), except that—after centrifugation and removal of the buffy coat—we performed only 2 washes (rather than 4) to remove residual extracellular Hb. We then resuspended RBCs in our oxygenated solution (see Table 2), alternatively, without any drug, with pCMBS (1 mM × 15 min), or with DIDS (200 μM × 1 h), to a final Hct of 25%. After centrifuging RBCs at 600 × g for 5 min, we aspirated and discarded the resulting supernatant to remove inhibitors. We then resuspended RBCs in our oxygenated solution to an Hct of 5% to 10%, centrifuged at 600 × g for 5 min, and performed 1 last wash. Finally, we either resuspended packed RBCs at ostensibly 50% Hct for automated hematological assays, or directed the RBCs to studies of flow-cytometry[18].

The above sequence is step #7–9 in Figure 1.

---

[17] See Methods>Preparation of RBCs>Processing of RBCs for assays 1–4

[18] See Paper #2>Methods>Flow cytometry>UseOfInhibInIFC

Estimation of thickness of biconcave disks (workflow #10)

As described in paper #3[19], we generate a torus that has a major outer diameter that matches the measured mean $Ø_{Major}$ of the RBC population (see above[20]), and has a volume that matches the measured mean MCV (see above[21]). We take the RBC thickness as the minor diameter of the torus.

The above sequence is step #10 in Figure 1.

Estimation of P_{M,O_2} to predict k_{HbO2} (workflow #11)

For our initial estimate of P_{M,O_2} in our macroscopic mathematical simulations, we assume that P_{M,O_2} in mouse RBCs has the same value as measured by Endeward *et al.* (2006) for the CO_2 permeability (P_{M,CO_2}) of human RBCs.

This estimation is step #11 in Figure 1. Further refinements lead (see steps #13 through #18, below) to slight adjustments to this value.

Determination of relative abundance (workflow #12)

As described in paper #2[22], we use imaging flow cytometry to determine the fraction of a cell population in our samples represented by various cell types, including BCDs vs. nBCDs.

---

[19] Paper #3>Methods>Mathematical modeling and simulations>Calculation of RBC thickness based on the geometry of a torus

[20] See Methods>Measurement of major cell diameter

[21] See Methods>Automated hematological analyses

[22] See Paper #2>Methods>Flow cytometry>Imaging flow cytometry (IFC)

This estimation is step #12 in Figure 1.

Macroscopic Mathematical Modeling (MMM) and simulation of HbO_2-deoxygenation time course, yielding k_{HbO_2} (workflow #13)

The details on the macroscopic[23] mathematical modeling and simulations are in paper #3[24]. In brief, we use a reaction-diffusion approach—based on a model originally developed for CO_2 fluxes across the membranes of *Xenopus* oocytes by Somersalo *et al.* (2012)—of O_2 efflux from an RBC that we model as a sphere with spherical-radial symmetry. Others have previously modeled RBCs as spheres (Vandegriff & Olson, 1984*a*; Williams & Kutchai, 1986; Deonikar & Kavdia, 2013; Deonikar *et al.*, 2014). These earlier workers took the sphere diameter to be the RBC major diameter. In contrast, the value that we assign to the sphere diameter ($Ø_{Sphere}$) is the RBC thickness (see above[25]).

As illustrated in Figure 2, the model system comprises (1) a spherical RBC; (2) a membrane that encompasses intracellular fluid (ICF); (3) O_2, Hb, and HbO_2 within the ICF; (4) a thin layer of extracellular unconvected fluid (EUF); and (5) an infinite reservoir of bulk extracellular fluid (bECF) that surrounds the EUF. Reactions among O_2, Hb and HbO_2 occur only in the ICF. We model the reaction term as the simple, one-step reversible reaction

---

[23] Distinguish between atomic (MD) and mesoscopic modeling vs. macroscopic (fine scale/electrode … coarse)

[24] See Paper #3>Methods>Mathematical modeling and simulations

[25] See Methods>Estimation of thickness of biconcave disks

$$HbO_2 \underset{k'}{\overset{k}{\rightleftharpoons}} Hb + O_2,$$

combined with a variation (see paper #3[26]) of the "variable rate coefficient" model proposed by Moll (1968), which guarantees that the hemoglobin-O_2 saturation curve is sigmoidal. All three solutes (i.e., O_2, Hb and HbO_2) diffuse within the cytosol. O_2 is the only solute that can move—via diffusion—through the plasma membrane, within the EUF and between EUF and bECF. Inputs to the simulations include (1) MCV and MCHC from automated hematological analyses (see above[27]), (2) the mean $Ø_{Major}$ of the BCDs (or non-BCDs) from imaging flow cytometry (see paper #2[28]), and (3) the rate constant of HbO_2 dissociation in an RBC lysate ($k_{HbO_2 \rightarrow Hb}$), which is equivalent to k in the above equation. Paper #3 contains details on the computational model,[29] parameter values,[30] and the simulation[31] of the time course of deoxygenation of HbO_2.

Based on the MMM, our use of the simulations to predict the time course of the reaction $HbO_2 \rightarrow Hb$ (and thus k_{HbO_2})—both for BCDs and non-BCDs—represent step #13 in Figure 1.

---

[26] See Paper #3>Methods>Mathematical modeling and simulations>Kinetics of the oxygen-hemoglobin reaction

[27] Methods>Automated hematological analyses (workflow #7-9)

[28] See Paper #2>Methods>Flow cytometry>Imaging flow cytometry

[29] Paper #3>Methods>Mathematical modeling and simulations>Computational model

[30] Paper #3>Methods>Mathematical modeling and simulations>Parameter values

[31] Paper #3>Methods>Mathematical modeling and simulations>Simulation of time course of HbO_2 deoxygenation, and estimation of k_{HbO_2}

Accommodation for nBCDs (workflow #14 through #19)

According to (1) our microvideography studies of RBCs on a coverslip, as visualized using an inverted microscopy, and (2) IFC, virtually all RBC samples comprise predominantly biconcave disks, but also may contain nBCDs. Although a nBCD ought to have the same intracellular total Hb content as a BCD, the intracellular diffusion distances are greater. Thus, the rate of O_2 offloading (see Figure 2) should be less for nBCDs than for BCDs. Thus, a mixture of BCDs and nBCDs will have an aggregate k_{HbO2} that is lower than the true k_{HbO2} of BCDs alone.

To arrive at the true k_{HbO2} for BCDs and extract the P_{M,O_2}, we accommodate for the shape change—that is, the presence of nBCDs—using the novel algorithm comprising steps #14 through #19 in Figure 1. The principle is straightforward: The time course of HbO_2 deoxygenation for a mixture of BCDs and nBCDs is the linear combination of the separate deoxygenation time courses of BCDs and nBCDs, each weighted for their relative numbers, as provided by imaging flow cytometry (see workflow #12). The MMM simulations, separate for both BCDs and nBCDs (see workflow #13) provide the first estimates of the time courses for HbO_2 desaturation for BCDs and nBCDs. The linear combination of these two time courses (workflow #14) yields the first estimate of the time course of the BCD-nBCDs mixture. Various algebraic manipulations (workflow #15-19), lead to a shape-correction factor that we can apply to each individual physiological experiment protocol (genotype ± inhibitors) to obtain an improved estimate of the true k_{HbO2} as well as an estimate for P_{M,O_2}. We present this algorithm paper #3[32].

[32] See Paper #3>Results>Accommodation for non-BCDs

Statistical analysis

We report results as mean ± SD. In each relevant figure legend, we report which statistical tests we performed, from among the following, to generate unadjusted *P*-values: (1) paired two-tailed t-test, or (2) one-way analysis of variance (ANOVA). For comparisons of 2 means, we performed #1. For comparisons among >2 means, we performed #2 and then, to control for type I errors across multiple means comparisons, we applied the Holm-Bonferroni correction (Holm, 1979), setting the familywise error rate (FWER) to $\alpha = 0.05$. Briefly, we order the unadjusted *P*-values for all $\mathcal{N}$ comparisons in each dataset from lowest to highest. For the first test, we compare the lowest unadjusted *P*-value to the first adjusted α value, $\alpha/\mathcal{N}$. If the null hypothesis is rejected, then we compare the second-lowest *P*-value to the second adjusted α value, $\alpha/(\mathcal{N}-1)$, and so on. If, at any point, the unadjusted *P*-value is ≥ the adjusted α, the null hypothesis is accepted and all subsequent hypotheses in the test group are considered null.

Data availability

The data supporting the findings of this study are available within the paper and its Supplementary Information files. Any further relevant data are available from the corresponding author upon reasonable request.

Results

In the present study, we use stopped-flow absorbance spectroscopy to monitor Hb deoxygenation as we mix oxygenated RBCs with a solution containing the O_2 scavenger sodium dithionite (final concentration, 25 mM). This NDT protocol virtually eliminates the effect of the EUF on O_2 efflux. We started by investigating the hypothesis that two small-molecule inhibitors (i.e., pCMBS, DIDS) block hypothetical O_2 channels. After evaluating the effects of genetic deletions of two major membrane proteins (i.e, AQP1, RhAG) on O_2 offloading from RBCs as part of this paper #1, we tested the hypotheses that observed effects on O_2 offloading could reflect changes of RBC geometry or changes in the abundance of major RBC membrane proteins as part of paper #2. Finally, the mathematical simulations in paper #3 provide a quantitative basis for interpreting the data in papers #1 and #2, elucidate the dependence of Hb deoxygenation on membrane O_2 permeability, and support the conclusion that two identified channel proteins as well as a third as-yet-unidentified protein account for nearly all of the O_2 permeability of murine RBCs.

Effect of pCMBS or DIDS on O_2 offloading from RBCs

Stopped-flow approach. As detailed in Methods, our general approach is to mix, in the reaction cell of the SF device, (1) RBCs (HCT ≅ 0.4%) suspended in our oxygenated solution (see Table 2) with (2) a deoxygenated solution containing sodium dithionite at a nominal concentration of 50 mM. In the reaction cell, the NDT, now at a nominal concentration of 25 mM, annihilates the extracellular O_2 in the reaction:

$$\underbrace{2Na^+ + S_2O_4^=}_{\text{NDT}} + H_2O + O_2 \rightarrow 2Na^+ + HSO_4^- + HSO_3^- \ .$$

The effect of this level of NDT in eliminating extracellular O_2 is so powerful that it is presumed to virtually eliminate the effect of the EUF ("unstirred layer") on O_2 efflux because $[O_2]_{EUF} \cong 0$ and thus extracellular O_2 has a negligible effect in slowing the net efflux of O_2 from the RBC (Huxley & Kutchai, 1981; Vandegriff & Olson, 1984*a*, 1984*b*, 1984*b*; Holland *et al.*, 1985).The

transmembrane O_2 gradient now favors O_2 efflux from the RBC, which in turn leads to the diffusion of free O_2 and HbO_2 from the bulk intracellular fluid to the inner face of the membrane and ultimately, throughout the cell, to the reaction $HbO_2 \rightarrow Hb + O_2$, which we assess by monitoring the absorbance spectrum of Hb.

Effect of pCMBS on O_2 offloading from RBCs. The 3D graph in Figure 3*A* shows an example of the time course of Hb absorbance spectra (see above[33]) of ostensibly intact, control RBCs harvested from WT mice. We refer to these cells as "ostensibly" intact because, although we took care to load into the SF device only what appeared to be intact RBCs (*Act%H* ≅ 0.37%; Zhao *et al.*, 2017), we will see that some fraction is lysed in the SF reaction cell; we introduce the accommodation for hemolysis in the next two paragraphs. These are "control" cells because we have not treated them with drugs. In parallel with the control cells in Figure 3*A*, in Figure 3*C* , we show the 3D graph for RBCs treated with pCMBS, a sulfhydryl reagent known to inhibit CO_2 diffusion through AQP1, either with AQP1 expressed *Xenopus* oocytes (Cooper & Boron, 1998), or with native AQP1 in human RBCs (Endeward *et al.*, 2006). From the data in Figure 3*A–B*, we compute the time courses of relative HbO_2 saturation (see above[34]). The records in Figure 3*C* show that pCMBS markedly slows the deoxygenation of Hb within ostensibly intact RBCs. From each such HbSat-vs.-time record, we obtain a "raw" k_{HbO_2} value (see above[35]), which we summarize for

---

[33] See Methods>Stopped-flow absorbance spectroscopy (workflow #1). The ">" symbol indicates that the level-2 heading "Stopped-flow absorbance spectroscopy (workflow #1)" is under the level-1 heading "Methods". It is understood that this reference is to a location in the present paper unless the callout is preceded by "Paper #2>" or "Paper #3>".

[34] See Methods>Calculation of time course of HbO_2 desaturation (workflow #2).

[35] See Methods>Calculation of "raw"-k_{HbO_2} (workflow #3)

paired control vs. pCMBS-treated RBCs in the first data row of the blue columns in Table 3*A*. Based on raw values, pCMBS reduces k_{HbO_2} by 57.7%.

As detailed below[36], we accommodate each "raw"-k_{HbO_2} value for the small amount of HbO_2 released into the bulk ECF by RBCs that lyse within the SF reaction cell. Because the released HbO_2 deoxygenates more rapidly than HbO_2 surrounded by the RBC membrane (Hartridge & Roughton, 1928), it leads to an overestimate of k_{HbO_2}. Thus, as summarized for ±pCMBS in the second data row of the blue columns in Table 3*A*, both hemolysis-corrected (HC) k_{HbO_2} values are lower than the corresponding raw values. Because the HC-k_{HbO_2} falls more for +pCMBS than for –pCMBS, the % inhibition by pCMBS rises somewhat to 63.2%.

Also as described below[37]—and as detailed in paper #3[38]—we additionally accommodate for the appearance of non-biconcave disks, which are rare among control cells but more common with pCMBS-treated and especially DIDS-treated cells. Because the mean diffusion distance is greater (slowing deoxygenation) in nBCDs than in BCDs, the shape-corrected (SC) values—summarized in the third data row of the blue columns in Table 3*A*—modestly exceed the corresponding HC-k_{HbO_2} values.

After accommodating for hemolysis and nBCDs, we conclude that pCMBS decreases k_{HbO_2} of intact BCDs by ~61% (Figure 3*E*).

---

[36] See Results>Accommodation for Hemolysis

[37] See Results>Accommodation for nBCDs

[38] See Paper #3>Results>Accommodation for nBCDs

Although pCMBS, with its sulfonate group, was designed to be membrane impermeant, a trivial explanation for the drug effects in Figure 3*D–E* is that pCMBS somehow gains entry into the RBC and, directly or indirectly, slows the reaction $HbO_2 \rightarrow Hb + O_2$. To determine whether pCMBS does indeed access the RBC cytosol, we use the RBC's endogenous, cytosolic carbonic anhydrase as a sentinel. Our CA assay is the same one we use for assessing hemolysis (see above[39]), namely, mixing two dissimilar CO_2/HCO_3^- solutions (see Table 2) in the SF reaction cell to create an out-of-equilibrium state that favors the reaction: $HCO_3^- + H^+ \rightarrow CO_2 + H_2O$ (↑pH), which is governed by the rate constant $k_{\Delta pH}$. The first bar in Figure 3*E* shows the $k_{\Delta pH}$ of the RBC lysate. The second bar shows that incubating the hemolysate with pCMBS for 15 minutes markedly reduces lysate CA activity. The last two bars show that treating intact RBCs with pCMBS, and then washing, does not significantly affect the $k_{\Delta pH}$ of the subsequent lysate (Figure 3*F*). Thus, we conclude that pCMBS—under the conditions of our experiments—does not significantly cross RBC membranes. Therefore, the ability of pCMBS to decrease k_{HbO_2} must reflect the action of the chemical from the extracellular side of the membrane.

Effect of DIDS on O_2 offloading from RBCs. Figure 4*A* and Figure 4*C* show representative time courses of Hb absorbance spectra of untreated and DIDS-treated RBCs from WT mice. Figure 4*D* shows time courses of relative HbSat, and reveals that DIDS markedly slows O_2 offloading (though not by as much with pCMBS). The first data row of the peach-colored columns of Table 3*A* summarizes paired "raw"-k_{HbO_2} values, and shows that DIDS lowers "raw"-k_{HbO_2} by ~35.6%.

---

[39] See Methods>Quantitation of hemolysis in SF reaction cell (workflow #4)

We accommodate these "raw"-k_{HbO2} values for the Hb released into the bulk ECF by RBCs lysed within the SF reaction cell, using an approach (see below[40]) that is a modification of the one that we employ for control and pCMBS-treated cells. We summarize these HC-k_{HbO2} values in the second data row of peach-colored columns in Table 3*A*. Although hemolysis correction lowers both k_{HbO2} values, it lowers the DIDS HC-k_{HbO2} to a greater extent, so that the DIDS inhibition rises to ~48.6%.

Finally, after accommodation for nBCDs, we see in the third data row of peach-colored columns in Table 3*A* that SC-k_{HbO2} rises slightly for the control cells but—because DIDS leads to more nBCDs formation—k_{HbO2} rises more substantially for DIDS-treated cells. After accounting for hemolysis and nBCDs, we conclude that DIDS reduces the SC-k_{HbO_2} by ~31.2% (Figure 4*E*).

To determine whether DIDS accesses RBC cytosol—and because DIDS (unlike pCMBS in Figure 3*F*) has little effect on CA activity (not shown)—we use cytosolic Hb as a sentinel. The left pair of bars in Figure 4*F* shows that incubating an RBC lysate with DIDS substantially reduces k_{HbO_2} of the lysate. However, the right pair of bars reveals no significant effect on k_{HbO_2} if we treat ostensibly intact RBCs with DIDS, then wash off the DIDS and, finally, form the lysate in the absence of DIDS. Thus, DIDS does not significantly cross RBC membranes. We conclude (as we did for pCMBS) that the ability of DIDS to decrease k_{HbO2} is a consequence of an action of the chemical on the extracellular side of the membrane.

Effect of genetic deletions on O_2 offloading from RBCs

Because our data reveal that neither pCMBS nor DIDS crosses RBC membranes to enter the cytosol (Figure 3*F* and Figure 4*F*), and because we are unaware of evidence that either pCMBS

[40] See Results>Accommodation for Hemolysis

(Vansteveninck *et al.*, 1965; Rothstein *et al.*, 1973) or DIDS interacts with the lipid component of RBC membranes (Cabantchik & Rothstein, 1974; Moriyama *et al.*, 2015), we reasoned that pCMBS and DIDS must reduce k_{HbO_2} by inhibiting membrane proteins that conduct O_2.

Effects of single and double knockouts. We began our search for such proteins by examining the time course of HbSat of RBCs from mice genetically deficient in AQP1 or RhAG, proteins with established roles as major CO_2 channels in human RBCs (Endeward *et al.*, 2006, 2008). Data from representative experiments show that the speed of O_2 offloading from Hb gradually decreases in the order WT > AQP1-KO > RhAG-KO > dKO (Figure 5*A*).

The four colored columns of Table 3*B* summarize "raw"-k_{HbO_2}, HC-k_{HbO_2}, and SC-k_{HbO_2}—under control conditions (i.e., absence of drugs)—for a larger number of mice, for each of the four genotypes. The magnitudes of the differences from row to row—"raw"- to HC- to SC-k_{HbO_2}—are rather small because both hemolysis and nBCDs abundance are rather small. The bar-graph summary in Figure 5*B* shows that the genetic deletion of AQP1 reduces SC-k_{HbO_2} by ~9%. The knockout of RhAG produces a decrease of ~17%, and the double knockout of AQP1 and RhAG lowers SC-k_{HbO_2} by ~30%. As summarized below[41] and detailed in paper #3, our mathematical simulations show that—because RBC dimensions, Hb content and concentrations, and Hb kinetics vary little among the four genotypes—the percent decreases in k_{HbO_2} correspond to far larger decreases in P_{M,O_2}, ~55% in the case of RBCs from dKO mice.

As described in paper #2[42], our proteomic analysis of RBC ghosts, which covers >1100 proteins, shows that the two single knockouts and the double knockout appropriately deplete the

---

[41] See Results> Mathematical simulations

[42] See Paper #2>Results>Proteomics

membranes of AQP1 and/or RhAG and Rhesus blood group D antigen (RhD). However, the two KOs or the dKO do not significantly affect the inferred abundance of any other RBC proteins among the top-ranked 100. Indeed, only 27 proteins (out of the >1100) exhibit a significant change in one of the KOs or the dKO, and these are proteins with relatively low inferred abundance. Of plasma-membrane–associated (PMA) proteins, the one with the highest inferred abundance to exhibit a significant change was ITGA2A, which ranked[43] #136 overall and #48 among PMA proteins. Of non-PMA proteins, the highest ranking[44] one with a significant change was PSMA4 (#101 overall). These two proteins had baseline inferred abundances <1% of the top-ranked protein, AE1 (i.e., SLC4A1). We conclude that it is highly unlikely that a change in the expression level of an off-target protein could account for our SC-k_{HbO_2} data.

Combined effects of dKO and pCMBS. We also examined the effect of pCMBS or DIDS on k_{HbO_2} in RBCs isolated from dKO mice. Figure 5*C* contains representative time courses of HbO_2 desaturation for RBCs from a dKO mouse, both under control conditions and after pre-treatment with pCMBS. It shows that O_2 offloading—already lower in RBCs from dKO vs. WT mice—slows even further after pCMBS.

The blue columns of Table 3*C* summarize paired "raw"-k_{HbO_2}, HC-k_{HbO_2}, and SC-k_{HbO_2} for RBCs from dKO mice, under control vs. pCMBS conditions. Figure 5*D* shows that, on a dKO background, pCMBS reduces SC-k_{HbO_2} by a further ~68%. Because the dKO by itself produced a ~30% decrease, this additional decrease caused by pCMBS corresponds to a ~78% overall

[43] See Paper #2>Table 9

[44] See Paper #2>Table 10

decrease in SC-k_{HbO_2}. Our mathematical simulations[45] indicate that this ~78% decrease in SC-k_{HbO_2} corresponds to a ~91% decrease in P_{M,O_2}.

Combined effects of dKO and DIDS. As illustrated in Figure 5*E* for representative paired experiments on a dKO background, DIDS slows the time course of HbO_2 desaturation, though not by as much as pCMBS.

The light-brown columns of Table 3*C* summarize paired "raw"-k_{HbO_2}, HC-k_{HbO_2}, and SC-k_{HbO_2} for RBCs from dKO mice, under control vs. DIDS conditions. Figure 5*F* shows that, on a dKO background—which by itself reduces SC-k_{HbO_2} by ~30% decrease—DIDS reduces SC-k_{HbO_2} by a further ~32%. This additional decrease caused by DIDS corresponds to a ~53% overall decrease in SC-k_{HbO_2}. Our mathematical simulations[46] indicate that this ~53% decrease in SC-k_{HbO_2} corresponds to a ~76% decrease in P_{M,O_2}.

Accommodation for Hemolysis

In a previous study in which we used the same methods as in the present study, the fraction of RBCs hemolyzed was ~0.37% before they enter the SF device, but ~5% while the cells were in the SF reaction cell (Zhao *et al.*, 2017). This increase presumably reflects the susceptibility of a subfraction of RBCs to the stress of the SF procedure, resulting in cell lysis and the release of HbO_2 into the bECF. We hypothesize that this released HbO_2, because it is not separated from the NDT by the RBC membrane, (1) deoxygenates faster than the HbO_2 within intact RBCs, leading to (2) an overestimate of k_{HbO_2}. If RBCs treated with inhibitors or isolated from KO mice have an

[45] See Results> Mathematical simulations

[46] See Results> Mathematical simulations

increased degree of hemolysis, we would underestimate the degree of inhibition. Therefore, for each RBC preparation from each mouse, we assayed hemolysis as outlined in Methods[47].

Hemolysis measurements

Effect of drug treatments on hemolysis. Figure 6*A* schematically illustrates our approach to accommodate for hemolysis measured inside the SF reaction cell (Zhao *et al.*, 2017). Figure 6*B* schematizes this approach to the control-cells (i.e., no drugs), Figure 6*C* schematizes this approach to the pCMBS-treated cells (i.e., pCMBS), Figure 6*D* schematizes this approach to the DIDS-treated cells (i.e., DIDS). Our analysis of hemolysis shows that, compared to control/WT RBCs (~5.2% hemolysis), those pretreated with pCMBS (~8.2%) or DIDS (~13.4%) exhibited a significant increase (Figure 6*E*). Note that we accommodate for hemolysis, as described below[48].

Effect of channel knockouts on hemolysis. Our analysis of the two KO sub-strains and the dKO reveal no significant difference in hemolysis compared to the WT (Figure 6*F*). These results are consistent with the report that deletion of *Rhd* and *Rhag* do not increase RBC fragility (Goossens *et al.*, 2010).

Among RBCs from dKO mice, we find that pretreatment with pCMBS or DIDS—as was the case for RBCs isolated from WT mice—produce significant increases in hemolysis. Moreover, on the dKO background pCMBS and DIDS produce somewhat greater degrees of hemolysis (Figure 6*G*) compared to the WT background (Figure 6*E*). Note that we accommodate for hemolysis, as immediately below.

---

[47] See Methods>Quantitation of hemolysis in SF reaction cell (workflow #4)

[48] See Results>Accommodation for hemolysis>Accommodation of "raw"-k_{HbO_2} …

Accommodation of "raw"-k_{HbO2} for hemolysis

We have developed two variants of a novel approach to accommodate for hemolysis in the SF reaction cell. The first variant applies to cells that are either not treated with a drug (i.e., controls) or pretreated with an agent(s) that does not appreciably affect the rate of the extracellular reaction $HbO_2 \rightarrow Hb + O_2$. The second variant applies to experiments in which the agent(s) (e.g., DIDS) does significantly affect this reaction.

Control or pCMBS-treated RBCs. Figure 7*A* shows the result of applying this approach (as illustrated in Figure 6*A*) to a representative control experiment (i.e., no drugs). In this figure, the blue x-axis is the apparent hemolysis, whereas the green x-axis is the actual hemolysis, measured as described in Methods[49]. One might unwittingly assume that the *Act%H* in SF reaction cell, is 0% (i.e., 100% of RBCs are ostensibly intact), and thus believe that the measured "raw"-k_{HbO2} of 3.70 s^{-1} in this experiment is in fact the actual "raw"-k_{HbO2}. However, the hemolysis assay in this example shows that *Act%H* is in fact 4.4% (shown on the green x-axis). To determine the actual "raw"-k_{HbO2} when *Act%H* truly is 0%, we mix 100% ostensibly intact RBCs (*Act%H* ≅ 4.4%) with 100% hemolyzed RBCs (*Act%H* = 100%) in increasing ratios, as shown by the blue points in Figure 7*B*. When we reference these blue points to the blue x-axis, we obtain a regression line that describes apparent "raw"-k_{HbO2} vs. *App%H*, with a slope of ~5.5256 s^{-1}/%*H* and a y-intercept of ~3.70 s^{-1} on the blue axes. To reference these same blue points to the green x-axis, we scale the x-axis and the slope of the regression line by the factor:

$$scaling\ factor = \left(\frac{100\%}{100\% - (Act\%H)_{App\%H=0}} \right) \approx \left(\frac{100\%}{100\% - (\sim 4.4\%)} \right) \approx 1.04566 .$$

[49] See Methods>Quantitation of hemolysis in SF reaction cell (workflow #4)

We also translate the green x-axis so that the measured *Act%H* (i.e., ~4.4%) lines up with the *App%H* of 0% on the blue x-axis. We calculate actual k_{HbO2} by back-extrapolating the regression line—now referenced to the scaled/translated green axes—to *Act%H* = 0. As illustrated in Figure 7*B*, here the y-intercept is ~3.45 s^{-1}, which represents the hemolysis-corrected k_{HbO2}.

We apply the above approach to the pCMBS-treated cells as schematized in Figure 6*C*, and exemplified in Figure 7*B*. Indeed we performed the hemolysis accommodation, as in Figure 7, for every experiment, save those in which we pretreated cell with DIDS.

DIDS-treated RBCs. As noted in Methods[50], for two reasons we must approach the accommodation for hemolysis somewhat differently in DIDS-pretreated RBCs than in control or pCMBS-treated cells. First, in 100%-hemolyzed RBCs, a 1-h pretreatment with DIDS markedly (~85%) reduces k_{HbO_2} (compare green and gray-blue bars in Figure 8*A*). The large difference in bar heights is relevant for RBCs as we load them into the SF device, when the fraction of hemolyzed cells is minute (i.e., *Act%H* ≅ 0.37%; see Zhao *et al.*, 2017), but the duration of drug exposure is sizeable. Second, during the actual SF experiment—and on a ms-to-s time scale—DIDS produces only a small (~4%) reduction in k_{HbO_2} (compare green and gray-blue open bars in Figure 8*B*). In this case, although the fractional inhibition is small, the fraction of Hb newly released in the SF reaction cell is much larger.

In the control RBCs in Figure 8*C*, the approach for obtaining the regression line is the same as in Figure 7*A*. Figure 8*C* shows the k_{HbO_2} hemolysis correction for RBCs—from 1 mouse—studied under control conditions (i.e., no DIDS). Here, $Slope_{Ctrl,Act}$ is 6.51 s^{-1}/*Act%H*.

---

[50] See Methods>Accommodation for hemolysis (workflow #5)>DIDS-treated RBCs

For the DIDS-treated cells in Figure 8*D*, we use a novel approach to obtain the regression line. In Methods, Eqn (1) describes (without a numerical example) the actual slope of this regression line. For RBCs from the same mouse as in Figure 8*C*, but treated ×1 h with 200 μM DIDS before entry into the SF device, the *Act%H* was 12.7% in the SF reaction cell. Inserting these %*H* values for this mouse—and the average k_{HbO2} for 7 mice in Figure 8*A*–*B*—into Eqn (1) yields:

$$Slope_{\mathrm{DIDS,Act}} = \underbrace{6.511\frac{\mathrm{s}^{-1}}{Act\%H}}_{Slope_{\mathrm{Ctrl,Act}}} \cdot \left[\underbrace{\underbrace{\underbrace{\frac{1.85\,\mathrm{s}^{-1}}{14.71\ \mathrm{s}^{-1}}}_{0.12576} \cdot \underbrace{\frac{0.37\%}{12.7\%}}_{0.031496}}_{0.00396} + \underbrace{\underbrace{\frac{13.52\ \mathrm{s}^{-1}}{14.03\ \mathrm{s}^{-1}}}_{0.96365} \cdot \underbrace{\frac{12.7\% - 0.37\%}{12.7\%}}_{0.96850}}_{0.933298}}_{0.937259} \right] = 6.114\frac{\mathrm{s}^{-1}}{Act\%H}.$$

Note that although this slope correction[51] amounts to only 100% – (~93.7%) = ~6%, it affords improved accuracy and shows that potential errors are not likely to be large. As summarized in Figure 8*D*, for this particular mouse[52]:

$$k_{\mathrm{HbO_2DIDS,Act}} = 2.348\,\mathrm{s}^{-1} - \left(6.114\frac{\mathrm{s}^{-1}}{Act\%H}\right) \cdot \left(12.7\%\,Act\%H\right) = 1.57\,\mathrm{s}^{-1}.$$

---

[51] Evaluating the above equation, as written, yields 6.11538, as opposed to 6.114. The discrepancy is due to rounding errors in the written equation.

[52] Evaluating the above equation, as written, yields 1.56, as opposed to 1.57. The discrepancy is due to rounding errors in the written equation.

Hematological and related parameters

We present the macroscopic mathematical model and simulations of O_2 offloading in paper #3. Below[53], in the present paper, we summarize elements of particular relevance to the present paper. It is perhaps intuitively obvious that k_{HbO_2} should decrease with (1) increases in MCV (due to increased diffusion distances) and (2) increases in MCHC (due to increased interactions between O_2 and Hb that slow effective O_2 diffusion), and (3) with decreased kinetics of HbO_2 dissociation. To evaluate potentially trivial explanations for the decreases in k_{HbO_2} observed in Figure 3, Figure 4, and Figure 5, we performed a series of hematological, morphometric, and HbO_2 kinetics studies.

Automated hematology

We performed a battery of assays (see Methods[54]) on the fresh blood of a large subset of mice used in the present study. In the largest group of such studies, we examined all four genotypes (Table 4). Because we observe no significant sex-related differences, we grouped the data from male and female mice (M+F). The only genotype-related differences that reach statistical significance are with RBCs from *Rhag*–/– and dKO mice, which for M+F exhibit slightly higher mean values for RDWa and MCV, but slightly lower values for MCHC .

The slightly higher RDWa values may correlate with the trend (not statistically significant) for KO mice, particularly RhAG-KO and dKO, to have higher percentages of reticulocytes and nucleated cells (see paper #2[55]). Regarding the increased MCV but decreased MCHC values, our

---

[53] See Results>Mathematical simulations

[54] See Methods>Automated hematological analyses (workflow #7–9)

[55] See Paper #2>table 3

mathematical simulations (see below[56]) indicate that these effects would tend to cancel. The bar graphs in Figure 9 summarize the most pertinent automated hematology data, including those with statistically significant differences (see Figure 9*B*, *D*, *F*).

For hematological studies with inhibitors (see Methods[57]), we generated preparations of RBCs from WT and dKO mice, and then pretreated these with no drug, pCMBS, or DIDS—a total of six conditions ([WT vs. dKO] × [control vs. pCMBS vs. DIDS]). Most of the statistically significant effects (Table 5) involve white blood cells or platelets, which the drugs generally tend to reduce in number. The effects on RBCs mainly involve MCV and MCHC, and these effects—as noted above regarding our mathematical simulations (see below[58])—are almost always in the directions that would tend to cancel vis a vis k_{HbO_2}.

The RBCs summarized in Table 5 include those blood samples that we used for the IFC studies in paper #2[59].

---

[56] See Results>Mathematical simulations

[57] See Methods>Automated hematological analyses (workflow #7–9)>Use of inhibitors in automated hematological studies

[58] See Results>Mathematical simulations

[59] See Paper #2>table 3

Morphometry

Blood smears. In paper #2[60], we present two sets of blood-smear data. In the first, we examined control cells (i.e., those not exposed to pCMBS or DIDS) of all four genotypes. The pathologist read the RBC morphology (see paper #2[61]) as "unremarkable, demonstrating only occasional target cells and stomatocytes, with no differences noted among knockout strains and WT mice."

In the second set of blood-smear data, we examined blood from (1) WT or (2) dKO mice pretreated with (a) neither pCMBS (controls), (b) with pCMBS, or (c) with DIDS (i.e., a total of 2 × 3 = 6). The pathologist read the RBC morphology (see paper #2[62]) as showing "no significant differences in red cell morphology … under any of the [six] conditions." The absence of a comment about increased nBCDs abundance in the drug-treated cells in the blood smears (where we plate, stain, and dry the cells after drug pretreatment) is interesting, inasmuch as nBCDs were apparent in images of living, tumbling RBCs or RBCs visualized by IFC.

Living RBCs tumbling through the focal plane of an inverted microscope. In paper #2, we also examine RBCs in suspension as we drop them onto a coverslip on the stage of an inverted microscope, and then image the cells as they fall through the focal plane. For control RBCs (no inhibitors present) of all four genotypes, the RBCs appear as normal biconcave disks,

---

[60] See Paper #2>Results>Morphometry>Blood smears

[61] See Paper #2>figure 1

[62] See Paper #2>figure 2

with occasional (~1.35%) poikilocytes, both in still images (see paper #2[63]) and video recordings (see paper #2[64]).

In a second set of studies, we similarly examined RBCs—untreated, pretreated with pCMBS, or pretreated with DIDS—from WT or dKO mice. Whereas the appearance of the control RBCs (no inhibitor) was again unremarkable, we observed spherical cells (sometimes with spicules)—"nBCDs"—in the pCMBS experiments, and more so in the DIDS experiments (see paper #2[65]).

Light-scattering flow cytometry. As presented in paper #2[66], these studies—which included the development of gating schemes (based on staining with fluorescent markers) to distinguish various cell types—showed that RhAG-KO and dKO mice have slightly larger and more varied RBC sizes compared to WT and AQP1-KO mice. However, the overall differences in cell size and shape among the genotypes were not significant.

Living RBCs visualized using imaging flow cytometry (IFC). In a fourth and final approach for assessing RBC morphometry—and as presented in paper #2[67]—we establish gating schemes and then obtain photographs of single cells as they fly before a microscope objective.

---

[63] See Paper #2>figure 3

[64] See Paper #2>Supporting Information

[65] See Paper #2>figure 4

[66] See Paper #2>Results>Morphometry>Light-scattering flow cytometry

[67] See Paper #2>Results>Morphometry>Imaging flow cytometry

Cell shape. We found that even control (not treated with inhibitors) RBCs from WT and dKO mice have ~2% nBCDs (see paper #2[68]). After pretreatment with pCMBS, the fraction increased significantly for the WT (~8.7%) but less so in the dKO (~5.7%). The pattern was the same following DIDS pretreatments, except that the fraction of nBCDs was far higher (41% for WT vs. 21% for dKO). The presence of nBCDs, particularly after drug pretreatment, led us to develop a novel approach to accommodate for these effects, as summarized below[69].

The decrease in nBCD abundance—both for samples pretreated with pCMBS or with DIDS (see previous paragraph)—in dKOs vs. WTs is consistent with the hypothesis that the drug-induced shape changes depend, at least in part, on interactions of the drugs with AQP1 and/or Rh_{Cx}.

Major RBC diameter ($Ø_{Major}$). The IFC experiments not only identify cell shape, but also provide—for cells with the proper orientation—the major diameter of BCDs and of nBCDs (see paper #2[70]). These values are an important input to the mathematical simulations (see below[71]).

Hb kinetics ($k_{HbO2 \rightarrow Hb}$)

To examine the possibility that the knockout of one or both channels could affect Hb kinetics, we determined k_{HbO_2} on 100% hemolyzed RBCs. The approach was the same as for 100% ostensibly intact RBCs (see Figure 3 and Figure 4), or for various mixtures of 100% ostensibly

---

[68] See Paper #2>figure 7

[69] See Results>Accommodation for nBCDs

[70] See Paper #2>table 6

[71] See Results>Mathematical simulations

intact and 100% hemolyzed RBCs (see Figure 7 and Figure 8). On the one hand, we find no significant differences among the mean $k_{HbO2 \rightarrow Hb}$ values for WT, AQP1-KO, RhAG-KO mice (Figure 10). However, we are somewhat surprised—inasmuch as the individual AQP1 and RhAG deletions were without effect—that the dKO produced a ~9% decrease of $k_{HbO2 \rightarrow Hb}$ (i.e., 100% lysate).

Because the reaction $HbO_2 \rightarrow Hb + O_2$ is only one of several processes that contribute to k_{HbO2}, intuition tells us that the ~9% decrease in $k_{HbO2 \rightarrow Hb}$ should account for even a smaller fraction of the ~30% decrease that we observed in dKO mice. Indeed, the sensitivity analysis in paper #3[72] indicates that a 9% decrease in $k_{HbO2 \rightarrow Hb}$ could account by itself for far less than half of the 9% k_{HbO2} decrease observed for AQP1-KOs, let alone the 30% decrease in dKOs.

Mathematical simulations

Our goal in the macroscopic mathematical modeling and simulations is not to adjust simulation parameter values to produce a MMM-k_{HbO2} (i.e., the simulated value) that matches the observed "raw"-k_{HbO2} (e.g., the control curve for WT RBCs in Figure 3*C*), but rather to predict—from first principles—the time course of hemoglobin desaturation (see paper #3[73]). The numerical inputs for our simulations (see paper #3[74]) are physical constants and other values taken from the

[72] See Paper #3>figure

[73] See Paper #3>Introduction

[74] See Paper #3>Methods>Mathematical modeling and simulations>Parameter values

literature[75] as well as genotype-specific values generated in the present studies[76]. Among the literature values, we took P_{M,O_2} to be 0.15 cm s^{-1} (workflow #11), the measured value of P_{M,CO_2} of Endeward *et al.*, (2006) in human RBCs. For the thickness of the unconvected layer, we chose 1 μm, which (given the high level of NTD in our experiments) may be an overestimate. Among genotype-specific values, the $Ø_{Major}$ (workflow #6, from paper #2[77]) and MCV (workflow #8 from paper #2[78]) are inputs for computing BCD thickness (workflow #10). MCV as well as MCH (workflow #7) together yield MCHC (workflow #9).

The result of our simulation for control WT RBCs (i.e, without inhibitors)—all cells assumed to be BCDs—is an MMM-k_{HbO_2} of ~3.99 s^{-1} (workflow #13; see paper #3[79]), which is analogous to a shape-corrected value in physiological experiments. For the data set summarized in Figure 3*D*, the mean SC-k_{HbO_2} value underlying the control/WT value (solid green bar) is 3.45 s^{-1}. For the (different) data set summarized in Figure 4*D* (solid green bar), the comparable value is 3.24 s^{-1}, and for Figure 5*B* (solid green bar), the value is 4.09 s^{-1}. Thus, our MMM-k_{HbO_2} value determined from first principles—3.99 s^{-1}—ranges from ~2.5% lower than the highest SC-k_{HbO_2} value to ~23% higher than the lowest value. We conclude that the MMM simulation provides a reasonable estimate of HbO_2 desaturation.

---

[75] See Paper #3>table

[76] See Paper #3>table

[77] See Paper #2>table 3

[78] See Paper #2>table 4

[79] See Paper #3>Results>Simulations of O_2 efflux

Accommodation for nBCDs

Because it appears that all RBC preparations comprise at least a small fraction of nBCDs, we developed a novel linear-combination method to accommodate for the presence of nBCDs (for summary, see Methods[80]; for details, see paper #3[81]). For our control/WT RBCs, the linear-combination procedure—which corrects for the presence of "slower" nBCDs (lower k_{HbO_2}) amidst the "faster" BCDs (higher k_{HbO_2})—raises the MMM-k_{HbO_2} value (i.e., ~3.99 s^{-1}, analogous to an "SC" value to the shape-corrected value of ~4.04 s^{-1}. We can then compute a shape-correction factor (i.e., ~ 4.04/3.99 ≅ 1.01), and apply it to any experiment on control/WT RBCs. Thus, if a particular mouse has an HC-k_{HbO_2} of 3.45 s^{-1}, the SC-k_{HbO_2} is ~3.48 s^{-1}. These shape-correction factors are small with control RBCs (WT or various KOs) but become larger with pCMBS or DIDS.

[80] See Methods>Accommodation for nBCDs (workflow #14 through #19)

[81] See Paper #3>Results>Accommodation for non-BCDs

Discussion

Overview

The combined results of the present paper and its two companion papers show that two channel proteins—AQP1 and the Rh complex—contribute ~55% of the O_2 permeability to murine RBCs. On the background of the AQP1/Rh_{Cx}-dKO, other protein(s) blocked by DIDS contribute an additional ~20% of P_{M,O_2}; proteins blocked by pCMBS contribute ~35%. If the DIDS-sensitive proteins (~20%) are a fully subset of the pCMBS-sensitive ones (~35%), then at least 90% of murine RBC O_2 traffic occurs via membrane channels under the conditions of our experiments. To the extent that a subset of DIDS-sensitive proteins in the dKO are not also pCMBS sensitive, O_2 channels would account for even more than 90% of the O_2 traffic.

Together with earlier CO_2 studies, the present work shows that, of the O_2 and CO_2 traffic across mammalian RBC membranes, at least 90% occurs through protein channels. Our work raises questions that should trigger new lines of research: What is the molecular mechanism of O_2 diffusion through the channels? We suggest that the most likely routes are the hydrophobic central pores at the middle of the AQP1 tetramers and Rh trimers, and/or other hydrophobic pathways between monomers. Which other membrane proteins contribute to P_{M,O_2} in RBCs? And to what extent do AQPs, Rh proteins, and other membrane proteins contribute to O_2 permeability in other cell types? An important implication of our O_2-channel work is that it provides a mechanism for cellular regulation of O_2 permeability by controlling the synthesis/trafficking of these channels, or by using post-translational modifications to modulate single-channel permeability. Our work raises the possibility of O_2-channelopathies in human disease. Finally, the O_2-channel paradigm offers the future physician the possibility of raising O_2 permeability (e.g., to enhance performance or wound healing) or lowering O_2 permeability (e.g., to treat oxygen toxicity) by altering the (1) number or (2) intrinsic permeability of channels.

A century ago, Krogh (1919) performed a mathematical analysis of O_2 off-loading from RBCs, which included not only dissociation of O_2 from Hb ($HbO_2 \rightarrow Hb + O_2$), but also the diffusion of O_2—lumped as a single process—through RBC intracellular fluid, across the RBC membrane to the bulk extracellular fluid of systemic capillary blood plasma, and then across the capillary endothelium, ultimately to the ICF of O_2-metabolizing cells (see paper #3[82]).

At the time, Krogh's analysis was a *tour de force* that blended state-of-the-art experimental physiology with mathematics. This mathematical approach, in the days before digital computational methods, required numerous simplifying assumptions to yield equations amenable to analytical solutions. Without these simplifying assumptions, Krogh's quantitative model—with its demonstrated great value to physiology—would have been impossible. Sixty years after Krogh, Kreuzer (1982) enumerated 15 implicit assumptions in the Krogh analysis, one of which implies that the RBC membrane offers no resistance to O_2 diffusion (i.e., $R_{M,O_2} = 0$). Whether or not Krogh himself would have agreed that R_{M,O_2} is, in fact, greater than 0, we suggest that his implicit assumption (i.e., $R_{M,O_2} = 0$) was a reasonable first step inasmuch as it enabled a mathematical analysis that provided the first quantitative insights into the Krogh cylinder. Nevertheless, this implicit assumption became dogma for at least a subset of physiologists. The present work, as discussed below[83], proves that the implicit assumption is incorrect.

A larger subset of physiologists have adhered to a very different idea: Overton's rule (a subset of the broader, previously proposed solubility-diffusion theory), which holds that the diffusion of substances across membranes depends exclusively on their solubility in the lipid phase of the membrane. At the time of Overton, the concept of a membrane protein's mediating transport

---

[82] See Paper #3>Discussion>Krogh

[83] See Discussion>Implications of the macroscopic mathematical model> Predictions for effects on P_{M,O_2}

across a membrane would have been entirely foreign. For most of the panoply of substances that cross cell membranes—water, inorganic ions, small molecules, and even large substances like fatty acids and prostaglandins—Overton's rule has long-since been abandoned in favor of channels and various transport proteins (for review, see Aronson *et al.*, 2017). The present work with the knockout and blockade of channels (see below[84]), together with previous work from this and other laboratories, provides further evidence that the narrow view—attributed by others to Overton—does not hold universally for gases. Rather, P_{M,O_2} in murine RBCs depends largely (~90%) on the presence and activity of at least three membrane proteins: AQP1, Rh_{Cx}, and at least one unidentified protein.

Automated hematology experiments

Our hematology assays (see Table 4 and Figure 9) did not reveal substantial differences among RBCs from mice of different genotypes, or of RBCs from WT or dKO mice treated with drugs. The critical values from the present paper for the mathematical simulations are MCV, MCH, and the derived MCHC (MCHC = MCH/MCV), all of which we passed along to paper #3 for simulations. We will see below[85] that KO-specific changes in MCV and MCHC tend to cancel out, leading to the conclusion that automated-hematology data cannot account for the genotypic effects on k_{HbO_2}.

---

[84] See Discussion>Implications of the macroscopic mathematical model> Predictions for effects on P_{M,O_2} & ..> Predicted effects of KOs on P_{M,O_2}

[85] See Discussion>Implications of the macroscopic mathematical model>Effect of channel knockouts on MCV and MCHC

In parallel with the two critical hematological parameters (MCV and MCHC), major diameter and nBCD abundance pass in parallel from paper #2 to paper #3, providing the final values required for the mathematical simulations and accommodations.

Stopped-flow experiments

Hemolysis. We developed our SF hemolysis assay (Zhao *et al.*, 2017), which is based on the release of CA from RBCs into the extracellular fluid, because we anticipated that some RBCs lyse within the SF reaction cell and thereby lead to an overestimate of k_{HbO_2}. In the present paper, we develop what we believe are the first approaches (Figure 7 and Figure 8) for accommodating for the hemolysis that must always be occurring during SF studies. In brief, we artificially create precise degrees of incremental hemolysis, measuring k_{HbO_2} at each. As predicted, k_{HbO_2} rises as apparent hemolysis rises. After a rescaling and translation to create an x-axis that represents actual hemolysis, a back-extrapolation yields the true k_{HbO_2} when actual hemolysis should be zero. Because this hemolysis-corrected k_{HbO_2} is always less than the "raw"-k_{HbO_2}, the fractional inhibition based on "raw"-k_{HbO_2} values will underestimate those based on HC-k_{HbO_2} values.

In the case of control RBCs (not treated with a drug), these hemolysis corrections are modest, in the range of 4.0% to 7.0% for WTs, 3.4% for AQP1-KOs, 5.3% for RhAG-KOs, and 9.8% to 10.7% for dKOs. For drug-treated cells, the corrections are larger, ~17% (pCMBS) and ~25% (DIDS) for WTs and 41% (pCMBS) and 33% (DIDS) for dKOs. The drug values are larger than their control counterparts because (1) the actual % hemolysis is larger than for control cells (see Figure 6) so that the extrapolation is somewhat greater and (2) drug-treated cells have lower "raw"-k_{HbO_2} values so that even the same absolute hemolysis correction produces a greater fractional change.

Non-biconcave disks (nBCDs). We developed our accommodation for nBCDs because we observed them in DIC images of living drug-treated RBCs (see paper #2[86]) Imaging flow-cytometry confirms that nBCDs—a mixture of poikilocyte types (mainly echinocytes, acanthocytes, and spherocytes)—appear in all of our preparations (see paper #2[87]). The abundance was extremely low in control RBCs from WT and dKO mice (~2%), larger with pCMBS pretreatment (~9% falling to ~5% in dKOs), and high in DIDS-treated cells (~40% falling to ~25% in dKOs). Because the delay between drug treatment and IFC experiments is greater (~30-90 min) than between drug treatment and SF experiments (~5 min), the nBCD abundance from IFC studies probably overestimates the actual abundance in SF studies.

To our knowledge, our IFC study is the first quantitative search in physiological experiments for nBCDs, which nevertheless were presumably present in previous studies. In future studies, it would be valuable to determine the interrelationships among (1) drug concentration and exposure time, (2) decrease in P_{M,O_2}, and (3) nBCDs abundance, with the goal of determining protocols that maximize inhibition while minimizing nBCDs formation.

In the present study, we accommodated for nBCDs by (1) using IFC data to obtain diameter and abundance, (2) assuming that the nBCDs are spheres, (3) assuming that membrane properties (e.g., P_{M,O_2}) and MCH (i.e., total amount of Hb/cell) are the same in BCDs and nBCDs, (4) using our mathematical simulations to make a provisional estimate of the k_{HbO2} of nBCDs (always lower

[86] See Paper #2>figure 4

[87] See Paper #2>figure 7

than for BCDs), and (5) applying our linear-combination approach (see paper #3[88]) to extract the k_{HbO_2} for BCDs (always higher than HC-k_{HbO_2}).

Note that although we assume that nBCDs are perfect spheres (minimal surface/volume ratio, slowest HbO_2 offloading), in fact nBCD surface geometry is often more complex (higher surface/volume, faster offloading). Thus, our k_{HbO_2} of nBCDs tends to be an underestimate so that our linear-combination approach tends to over-correct and yield a deduced k_{HbO_2} of BCDs—the SC-k_{HbO_2}—that overestimates the true k_{HbO_2} of BCDs. As a result, when computing fractional inhibition, we tend to underestimate very slightly the effect of channel KOs, and underestimate more substantially the inhibition produced by pCMBS and particularly DIDS.

In the case of control RBCs (not treated with a drug), both WT and KO, shape-change corrections (probably slight overestimates) are small, ~1%. In the case of drug-treated cells, the corrections (probably greater overestimates) are larger, ~6% for pCMBS and ~35% for DIDS. A consequence of the shape correctsions—even if we knew the surface/volume ratio of nBCDs with precision—is that calculations of fractional inhibition based on HC-k_{HbO_2} values will overestimate those based on SC-k_{HbO_2} values.

Overall assessment of accommodations. For control RBCs of all genotypes, the rate of hemolysis is small (*Act%H* ≅ 5%), the k_{HbO_2} correction for hemolysis is similarly small (~4% to ~7%), nBCDs abundance is low (~2%), and the additional correction for nBCDs is similarly small (~1%). We regard both our hemolysis assay and hemolysis correction as quite robust. Even so, the correction is likely to be most reliable with low *Act%H*. The shape-change correction is likely most reliable with now nBCDs abundance. Thus, we have our highest degree

---

[88] See Paper #3>Results>Accommodation for non-BCDs>Linear combination of hemoglobin-deoxygenation time courses

of confidence in our control data on RBCs from WT, AQP1-KO, RhAG-KO, and dKO mice—that is, the dKO likely reduces P_{M,O_2} by ~55%.

For WT and dKO cells pretreated with pCMBS, hemolysis is still modest (Act%H ≅ 8%), the k_{HbO2} hemolysis correction is modest to large (about –17% and –41%, respectively), nBCDs abundance is modest to small (~9% and ~5%, respectively), and the correction for nBCDs is small (about +6% in our favor, the hemolysis and shape corrections are in opposite directions. Thus, we have a high degree of confidence that pCMBS reduces P_{M,O_2} substantially, with best estimates of ~61% in RBCs from WT mice, and an additional ~17% on a dKO background.

WT and dKO cells pretreated with DIDS are the most problematic. Hemolysis is rather high (*Act%H* ≅ 13%), the k_{HbO2} hemolysis correction is high (about –25% and –33%, respectively), nBCD abundance is high (~40% and ~25%, respectively), and the correction for nBCDs is high (about +35%). Again, in our favor, the corrections are nearly equal but opposite. As a result, we have moderate confidence that DIDS reduces P_{M,O_2} substantially (though not as substantially as pCMBS), with best estimates of ~31% in RBCs from WT mice, and an additional ~22% on a dKO background.

Mechanism of drug action. Our work shows that neither pCMBS (see Figure 3*E*) nor DIDS (Figure 4*E*) gains significant entry to the RBC cytosol. Thus, the effects of pCMBS (a sulfhydryl reagent) and DIDS (an amino-reactive agent) must be at the level of the plasma membrane. Other authors have presumed that both drugs—neither of which is specific for one target—act on membrane proteins (Rothstein *et al.*, 1973; Cabantchik & Rothstein, 1974), and we know of no evidence that either interacts with membrane lipids (Vansteveninck *et al.*, 1965; Rothstein *et al.*, 1973; Cabantchik & Rothstein, 1974). Moreover, if either did interact with membrane lipids, we expect that the result—if any—would be to decrease the barrier to O_2 diffusion. Thus, the inhibitor data led us to explore channel KOs.

Effects of KOs on drug susceptibility. Although neither pCMBS nor DIDS is specific for a single target, AQP1 and Rh_{Cx} appear to be targets of each. Macey and Farmer (1970) were the first to show that mercurials reduce the water permeability of RBCs (for early review, see Macey, 1984). After the identification of AQP1 as the first H_2O channel, Preston *et al.* (1993) created the C189S mutation and demonstrated that the inhibitory effect of mercury on the H_2O permeability of AQP1 depends specifically on the interaction with Cys-189 (Preston *et al.*, 1993). Moreover, the mutation AQP1-C189S eliminates the ability of pCMBS to reduce P_{M,CO_2} (Cooper & Boron, 1998). Preliminary work suggests that DIDS also reduces the CO_2 permeability AQP1, as expressed in oocytes (Musa-Aziz *et al.*, 2007*b*, 2007*a*).

In the present study, our mathematical simulations (see paper #3[89]) suggest that, on a WT background, pCMBS reduces P_{M,O_2} by ~82%. On the other hand, on a dKO background, the drug decreases P_{M,O_2} only by ~91% – ~55% = ~36% (i.e., inhibition reduced by 56% on dKO background). For DIDS, the two degrees of inhibition for SC-k_{HbO2} are ~56% on a WT background, and ~76% – ~55% = ~21% on a dKO background (i.e., inhibition reduced by 63% on dKO background). Thus, the absence of AQP1 and Rh_{Cx} reduces the susceptibility of P_{M,O_2} to each drug by a substantial amount. We have already seen that (compared to a WT background) the dKO background reduces the susceptibility of RBCs to nBCD formation (see paper #2[90]). Thus, both from the perspective of P_{M,O_2} reduction and nBCD formation, both AQP1 and Rh_{Cx} appear to be major—although not the exclusive,—targets of both pCMBS and DIDS .

---

[89] See Paper #3>table

[90] See Paper #2>figure 7bc

Implications of morphometry and proteomics experiments

Morphometry. We were reassured to see that, for all three KO genotypes, the control cells—as for the WTs—were overwhelmingly shaped as biconcave disks (see paper #2[91]). Therefore, on the basis of RBC morphology alone, we conclude that we have no reason to be suspicious of the genotype-dependent decreases in SC-k_{HbO2} and inferred P_{M,O_2} and the deduction—independent of any inhibitor data—that AQP1 and Rh_{Cx} can be conduits for O_2.

In the absence of inhibitors, nBCD abundance detected by IFC in WTs and dKOs was <2% (see paper #2[92]); our linear-combination accommodations ought to be most reliable for these control cells (see paper #3[93]). For cells treated with pCMBS, nBCD abundance is still modest and we believe that our accommodation (i.e., SC-k_{HbO2}) is likely to be nearly as reliable as for control cells. For cells treated with DIDS, which produces smaller k_{HbO2} inhibitory effects than does pCMBS but a much larger nBCD abundance, we have a lesser degree of confidence in the accuracy of SC-k_{HbO2} and deduced the P_{M,O_2}. Nevertheless, even if we were to ignore the DIDS data, the overall conclusions of our three papers would be unchanged. That is, besides AQP1 and RhCx (the support for which comes from KO data on control cells), we conclude that RBCs have at least one additional pCMBS-sensitive conduit accounts for ~35% of P_{M,O_2}. If we accept the DIDS SC-k_{HbO2} values at face value, at least one additional DIDS-sensitive conduit accounts for ~21%.

Measurements of major diameter and nBCD abundance flow from paper #2 are used for mathematical simulations and accommodations in paper #3. Because of the large number of cells

---

[91] See Paper #2>figures 1–4 & 7. Also see Suppl_Video_1--WT

[92] See Paper #2>figure 7

[93] See Paper #3>Results>Accommodation for non-BCDs

on which we made measurements by IFC (paper #2[94]), we have high confidence in both measurements.

Proteomics. Our proteomics analysis shows that the genetic deletions of AQP1 and RhAG appropriately eliminated those proteins (plus RhD in the case of the RhAG-KO), but had no significant effect on the apparent abundance of any other proteins among those ranked in the top 100 of greatest inferred abundance (see paper #2[95]). Thus, the most straightforward explanation for our genotype-base data on RBCs is that it was the absence of AQP1 or RhCx per se that was responsible for the KO-induced decreases in SC-k_{HbO2} and deduced P_{M,O_2}.

Implications of the macroscopic mathematical model

The sphere. We model the RBC as a sphere, the diameter of which is the same as the calculated thickness of the RBCs used in physiological experiments. Thus, our approach emphasizes the free edge of the BCD, which contains most of the HbO_2. Others also have regarded BCD thickness as the dimension most relevant for diffusion (Roughton, 1932; Ponder, 1948; Forster, 1964; Endeward, 2012).

Simulated k_{HbO2} for control/WT RBCs. Our simulations—based on physical constants and values provided either by the literature or our own measurements on control RBCs from WT mice—produce an SC-k_{HbO2} value of 4.04 s^{-1}, which is within the range of our physiologically observed values obtained in different data sets (i.e., 3.24 s^{-1} in Figure 4*E*, 3.45 s^{-1} in Figure 3*E*, 4.09 s^{-1} in Figure 5*D*). This range of physiological SC-k_{HbO2} values reflects variations in the potency of the manufacturer-supplied NDT supply, with low potency (i.e., lower effective [NDT])

---

[94] See Paper #2>table 5

[95] See Paper #2>Results>Proteomics

generating a greater effective unconvected layer around the RBCs (Vandegriff & Olson, 1984*b*), and thus a lower apparent k_{HbO2} value (see paper #3[96]). We presume that our highest-observed SC-k_{HbO2} value reflects our most potent batch of NDT[97] and thus our most reliable estimate of a reference SC-k_{HbO2} for control/WT RBCs of our C57BL/6_{Case} mouse strain. This value of 4.09 s^{-1} also is closest to our simulated value of 4.04 s^{-1}.

In our studies with pCMBS (e.g., see Figure 3) and with DIDS (e.g., see Figure 4), we always examined RBCs, ±inhibitor, from the same mouse on the same day, thereby minimizing effects of NDT potency.

Predictions for effects on P_{M,O_2}. Starting with the simulation in which we assumed a P_{M,O_2} of 0.15 cm s^{-1}—this yielded the SC-k_{HbO2} value of 4.04 s^{-1} noted above—we systematically varied P_{M,O_2} in a series of nearly 75 simulations. The result is a sigmoidal dependence of k_{HbO2} on log(P_{M,O_2}), as shown in paper #3[98]. The highest simulated P_{M,O_2} is ~26.6 cm s^{-1}, which is near the asymptote of SC-k_{HbO2} ≅ 6 s^{-1}, corresponds to a situation in which we replace the membrane with an equivalent thickness of water. Thus, simulating a physiological SC-k_{HbO2} of 4.04 s^{-1} requires that we reduce the P_{M,O_2} of a "water membrane" by a factor of (26.6/0.15) ≅ 177. These data are inconsistent with the implicit assumption of Krogh that membranes, including RBC membranes,

---

[96] See Paper #3>figure

[97] For our current SF experiments, we purchase as many as 10 sealed glass bottles of NDT, and open them one at a time until we find one that has a powdery NDT-gas interface. The other bottles, which have a film or crust at the surface (due to NDT that has reacted with O_2 and H_2O), we discard.

[98] See Paper #3>figure

offer no resistance to O_2 diffusion.In fact, RBC membrane, even with a full complement of O_2 channels, offer a tremendous resistance to O_2 diffusion.

Figure 11 is a transformation of the data in the aforementioned sigmoidal curve in paper #3[99]. Here in Figure 11 we show how "% decrease of SC-k_{HbO2}" depends on the imposed "% decrease in P_{M,O_2}". At the lower left, the "WT" control point confirms that 0% decrease in permeability (P_{M,O_2} = 0.15 cm s^{-1}) yields 0% decrease of k_{HbO2} (k_{HbO2} = 4.04 s^{-1}). The point at the upper right confirms that a 100% decrease in permeability (P_{M,O_2} = 0) fully blocks O_2 offloading (k_{HbO2} = 0). Between these two extremes are points that represent the key results of the present paper. For example, simulating the ~30% decrease in SC-k_{HbO2} that we observe with RBCs from dKO mice requires that we reduce the P_{M,O_2} from its reference value of 0.15 cm s^{-1} by a further 55%. Matching the ~78% SC-k_{HbO2} decrease observed for dKO+pCMBS requires that we reduce P_{M,O_2} (from reference of 0.15 cm s^{-1}) by 91%. If gas permeability depended only on the solubility of the gas in the lipid phase of the membrane, as suggested by proponents of Overton's rule, all the points in Figure 11—with the y-axis values chosen to match our SC-k_{HbO2} values—would overlay one another at the origin. This is clearly not the case. Thus, Overton's rule, at least as applied to the O_2 permeability of our murine RBCs under our experimental conditions, must be false.

Predicted effects of KOs on deduced P_{M,O_2} values. One way of evaluating the internal consistency of our macroscopic mathematical model and resulting simulations is to ask whether the decreases in P_{M,O_2} predicted in Figure 11 for the individual channel knockouts sum to the same value as for the double knockout:

[99] See Paper #3>figure

$$
\begin{array}{ccccc}
(\Delta P_{M,O_2})_{\mathbf{AQP1\text{-}KO}} & + & (\Delta P_{M,O_2})_{\mathbf{RhAG\text{-}KO}} & \overset{?}{=} & (\Delta P_{M,O_2})_{\mathbf{dKO}} \\
\underbrace{(-21.6\%) \quad + \quad (-36.4\%)}_{58.0\%} & & & \cong & (-55.2\%)
\end{array} \quad . \tag{2}
$$

The agreement is good, with the individual KOs summing to a predicted P_{M,O_2} decrease of ~58%, modestly above the observed dKOs value of ~55%. We conclude that the model, as tested by physiological data, is well behaved.

Sensitivity analysis

Paper #3[100] presents an analysis of the sensitivity of the simulated k_{HbO2} to changes in eight different parameters. Our general conclusion is that no reasonable change in any parameter could account for our k_{HbO2} data on control RBCs from KO mice, let alone from inhibitor-treated RBCs from dKO mice. More specifically, k_{HbO2} is: (1) only modestly sensitive to $k_{HbO2>O2}$, which is a measured parameter; (2) only mildly sensitive to changes in [total Hb], which also is a measured parameter; (3) very modestly sensitive to changes in O_2 diffusion constants and virtually insensitive to changes in Hb and HbO_2 diffusion constants; and (4) moderately sensitive to changes in either the thickness of the unconvected layer (l) or the diameter of the sphere that, in the MMM, emulates $Ø_{Major.}$ Because the simulations deal with a single cell with no extracellular hemoglobin, the results are, by definition, both hemolysis- and shape-corrected

Effect of channel knockouts on MCV and MCHC

In our broadest automated-hematology data set (see Table 4), the knockouts involving RhAG (RhAG-KO and dKO) were associated with a statistically significant increases in MCV and reciprocal decreases in MCHC; the AQP1-KO data trended in the same direction. In a narrower

[100] See Paper #3>figures

data subset restricted to mice used in IFC studies—and then in mathematical simulations—these patterns of MCV and MCHC persisted as trends but did not reach statistical significance (see paper #2[101]).

MCV. Our imaging–flow-cytometry studies indicate that the aforementioned increases in MCV are mainly attributable to an increased abundance of immature cell types (see paper #2[102]), consistent with increased RBC production. Because both AQP1 and Rh_{Cx} are important components of the ankyrin complex (Vallese *et al.*, 2022), one might think that the deletion of one or both channels might impact RBC deformability, which in turn could lead to a decrease in average RBC lifespan, consistent with our observation of increased immature cell types. One might also think that the deletions could increase RBC fragility. However, we did not observe genotype-related differences in hemolysis within the SF reaction cell (see Figure 6*B*; Lauf & Joiner, 1976; Ballas *et al.*, 1984; Mathai *et al.*, 1996)

MCHC. Whereas the genetic deletion of one or both channels tends to raise MCV, the effect on MCH is virtually nil (see Table 4). As a result, MCHC—that is, the ratio MCH/MCV—tends to fall as MCV rises. The parameter-sensitivity analysis in paper #3[103] indicates that, all else (including $[Hb_{tot}]_i$) being equal, increases in the sphere diameter (a surrogate for RBC thickness,

---

[101] See Paper #2>table 4, which is a subset of the larger data set in Table 4 (in paper #1) and is restricted to the mice used in the experiments on imaging flow cytometry and the mathematical simulations. Although the numbers of observations are smaller, the trends are similar

[102] See Paper #2>table 3

[103] See Paper #3>Results>Mathematical simulations exploring the predicted sensitivity of k_{HbO2} to eight key kinetic and geometric parameters

which is related to MCV) used in the mathematical model causes MMM-k_{HbO2} to fall rather steeply[104]. On the other hand, the sensitivity analysis also shows that decreases in $[Hb_{tot}]_i$, all else (including sphere diameter) being equal, causes MMM-k_{HbO2} to rise rather steeply[105]. Intuitively, one might think that the two effects—↑MCV and ↓MCHC—would tend to cancel, a hypothesis that we address in the next paragraph.

Simulations based on genotype-specific data. To address the above hypothesis, in paper #3 of this series, we perform a set of mathematical simulations in which we mimic control cells (i.e., not pretreated with inhibitors) of all four genotypes. The input parameters are genotype-specific values of MCV, MCHC, and $Ø_{Major}$. This analysis[106] predicts that the AQP1-KO would actually increase SC-k_{HbO2} by ~1% (vs. the observed 9% decrease in Figure 5). The simulated SC-k_{HbO2} for the RhAG-KO is down by ~4% from WT vs. the observed ~17% decrease, and that for the dKO is down by ~4% from WT vs. the observed ~30% decrease. We conclude that the effects of anti-parallel (1) increases in MCV and (2) decreases in MCHC do indeed tend to cancel, and that variations in RBC dimensions and $[Hb_{tot}]_i$ cannot account for our SC-k_{HbO2} data among the four genotypes in the present study.

---

[104] See Paper #3>Results>Mathematical simulations exploring the predicted sensitivity of k_{HbO2} to eight key kinetic and geometric parameters>Effect of varying geometric parameters on k_{HbO2}

[105] See Paper #3>Results>Mathematical simulations exploring the predicted sensitivity of k_{HbO2} to eight key kinetic and geometric parameters>Effect of varying $[Hb_{tot}]_i$ on k_{HbO2}

[106] See Paper #3>Results>Mathematical simulations exploring genotype-specific values of MCV, MCHC, and $Ø_{Major}$

Acknowledgements

We thank Jean-Pierre Cartron for the gift of *Rhag*–/– mice, and for most helpful discussions. We thank Seong-Ki Lee for developing an improved approach for genotyping the *Rhag*–/– mice. The authors gratefully acknowledge Daniela Calvetti and Erkki Somersalo for having developed the engine of an earlier version of the CO_2/pH reaction-diffusion model of an oocyte, which in part served as the starting point for the RBC model. We also thank Thomas Radford for organizing the husbandry of the mouse colonies; Gerald Babcock for his role as laboratory manager; James W. Jacobberger and Philip G. Woost of the CWRU Flow Cytometry and Imaging Microscopy Core (FCIMC) for their assistance with flow cytometry; Daniela Schlatzer of the CWRU Center for Proteomics and Bioinformatics for their assistance with mass spectrometry. This work was supported by Office of Naval Research (ONR) grant N00014-11-1-0889, N00014-14-1-0716, and N00014-15-1-2060; a Multidisciplinary University Research Initiative (MURI) grant N00014-16-1-2535 from the DoD, NIH grant multi-scale modeling grant 5U01GM111251 (to WFB), and NIH grant R01 HL160857 (to WFB). R.O. and the modeling were supported in part by NIH grant K01-DK107787. R.R.G was supported by a fellowship grant from the ONR (N00014-12-1-0326). W.F.B. gratefully acknowledges the support of the Myers/Scarpa endowed chair.

Tables

Table 1. C57BL/6$_{Case}$ mice Genetic background analysis, based on ~10,000 single-nucleotide polymorophisms*

Character / Genotype	C57BL/6J	C57BL/6N	C57BL/6Group	Total
Aqp1+/+Rhag+/+	17.60 ± 0.89 %	18.85 ± 1.35 %	23.80 ± 0.00 %	60.25 %
Aqp1–/–	16.57 ± 1.49 %	19.40 ± 0.00 %	28.60 ± 0.00 %	64.57 %
Rhag–/–	22.77 ± 1.43 %	19.40 ± 0.00 %	28.60 ± 0.00 %	70.77 %
Aqp1–/–Rhag–/–	21.38 ± 3.20 %	24.73 ± 2.61 %	21.42 ± 5.85 %	67.53 %
Average	19.58 %	20.60 %	25.60 %	65.78 %

*N is 6 for each group, values represent mean ± SD.

Table 2. Physiological solutions*

Solution / Component or parameter	Oxygenated solution (also, RBC washing)	De-oxygenated solution	Components for OOE Hemolysis assay			Solutions for preparation of mouse erythrocyte ghosts		
			$\mathcal{A}$	$\mathcal{B}$	Mix†	Sedimentation Buffer	Wash Buffer	Lysis Buffer ‡
NaCl (mM)	92.5	15	140	116	128	150	150	0
KCl (mM)	0§	0§	3	3	3	0	0	0
$CaCl_2$ (mM)	0.01	0.01	2	0	1	0	0	0
Na_2HPO_4 / NaH_2PO_4 (mM)‖	44.89/13.11	44.89/13.11	0	0	0	4.06/0.94	0	0
HEPES (mM)	0	0	16	0	8	0	0	0
$NaHCO_3$ (mM)¶	0	0	~0	44	22	0	0	0
CO_2 (%)	0	0	~0	~1	0.5	0	0	0
pH	~7.40‖	~7.40‖	7.03#	8.41¶	~7.25	~7. 5‖	~7.0	~8.0
Pyranine (μM)Δ	0	0	0	2◊	1◊	0	0	0
RBCs or lysate	++	0	++▽	0	+▽	+	+	+
NDT♦	0	50	0	0		0	0	0
Tris-HCl (mM)	0	0	0	0	0	0	0	5
Dextran500(w/v)	0	0	0	0	0	0.75%	0	0
Temperature (°C)	RT	RT	10	10	10	RT	RT	RT
Osmolality (mOsm)	~300	~300	~295	~300	~298	_	~290	_

*This table shows the compositions of all the solutions used in either the present paper (1st in the series of 3) or the following paper (2nd of 3). The only solution in common with the two papers is the "Oxygenated solution". The "Deoxygenated solution" and the three "OOE" solutions ("A", "B", and "Mix") were used only in the present paper. The three "Solutions for the preparation of mouse erythrocyte ghosts" were used only in the following paper.

†The values in this "Mix" column are those at the instant of mixing solutions A and B (Zhao *et al.*, 2017). The solution is out of equilibrium because the pH of 7.25 is far too low for the system to be in equilibrium,

given [HCO_3^-] = 22 mM and CO_2 = 0.5%. Note that both solutions “A” and “B” were equilibrated with room air and are thus oxygenated.

[‡]Complete protease inhibitor tablet (Roche) – only for lysis and first wash following lysis step.

[§](Coin & Olson, 1979) previously used 0 mM KCl in this solution.

[‖]The ratio [$HPO_4^=$]/[$H_2PO_4^-$] determines the pH at RT (~22°C).

[¶]The addition of HCO_3^- generates a trivial amount of CO_2 and also some $CO_3^=$, and spontaneously yields a pH of 8.41 at 10°C.

[#]We titrated HEPES free acid (pK ~7.41) to pH 7.03 with NaOH at 10°C.

[Δ][Pyranine] in the reaction cell was either 1 μM (to obtain pH data) or 0 μM (to obtain background data).

[◊]In the hemolysis assay, when determining the background for the fluorescence signal, we omitted the pyranine dye.

[▽]In the hemolysis assay, when determining the uncatalyzed rate constant (k_{uncat}) of the reaction $HCO_3^- + H^+ \rightarrow CO_2 + H_2O$, we omitted RBCs and lysate.

[♦]NDT is freshly added and used within ~1 h. Final [NDT] in SF reaction cell is 25 mM.

Table 3. Summary of "raw", hemolysis-corrected, and shape-corrected k_{HbO_2} values

A. k_{HbO_2} of RBCs from WT mice, ±inhibitors

Condition / Parameter	Ctrl	pCMBS	*P* value	Ctrl	DIDS	*P* value
"raw"-k_{HbO_2} (s^{-1})	3.74 ± 0.31	1.81 ± 0.39	5.89×10^{-8}	3.56 ± 0.30	2.38 ± 0.12	1.08×10^{-6}
HC-k_{HbO_2} (s^{-1})	3.42 ± 0.25	1.26 ± 0.19	4.97×10^{-7}	3.21 ± 0.27	1.65 ± 0.19	3.84×10^{-8}
SC-k_{HbO_2} (s^{-1})	3.45 ± 0.25	1.34 ± 0.20	7.03×10^{-7}	3.24 ± 0.27	2.23 ± 0.26	1.07×10^{-6}
N	8			8		

Values represent mean ± SD. HC- k_{HbO_2}, hemolysis-corrected k_{HbO_2}; SC- k_{HbO_2}; shape-corrected k_{HbO_2}. For each comparison we use paired two-tailed t-test.

B. k_{HbO_2} of RBCs from WT and knockout mice

Condition / Parameter	WT	*Aqp1–/–*	*Rhag–/–*	*Aqp1–/–Rhag–/–*
"raw"-k_{HbO_2} (s^{-1})	4.22 ± 0.51	3.81 ± 0.32	3.56 ± 0.21	2.99 ± 0.23
HC-k_{HbO_2} (s^{-1})	4.05 ± 0.48	3.68 ± 0.29	3.37 ± 0.15	2.80 ± 0.23
SC-k_{HbO_2} (s^{-1})	4.09 ± 0.49	3.73 ± 0.30	3.41 ± 0.15	2.84 ± 0.24
N	10	12	10	11

Values represent mean ± SD. HC- k_{HbO_2}, hemolysis-corrected k_{HbO_2}; SC- k_{HbO_2}. shape-corrected k_{HbO_2} For Table 3B, we use one-way ANOVA with Holm-Bonferroni post-hoc means comparison for the mean Raw k_{HbO2} values (shown in "Statistic Tables" Table 3 B1), the mean hemolysis-corrected k_{HbO2} (HC-k_{HbO2}) values (shown in "Statistic Tables" Table 3 B2), and the mean shape-corrected k_{HbO2} (SC-k_{HbO2}) values (shown in "Statistic Tables" Table 3 B3) of all four mouse strains.

C. k_{HbO_2} of RBCs from double-knockout mice, ±inhibitors

Condition / Parameter	Ctrl	pCMBS	*P* value	Ctrl	DIDS	*P* value
"raw"-k_{HbO_2} (s^{-1})	2.90 ± 0.13	1.37 ± 0.06	3.47×10^{-10}	2.75 ± 0.30	2.20 ± 0.12	3.24×10^{-4}
HC-k_{HbO_2} (s^{-1})	2.59 ± 0.18	0.81 ± 0.23	3.99×10^{-9}	2.48 ± 0.33	1.47 ± 0.23	3.44×10^{-5}
SC-k_{HbO_2} (s^{-1})	2.63 ± 0.18	0.84 ± 0.24	4.96×10^{-9}	2.52 ± 0.34	1.70 ± 0.27	2.30×10^{-4}
N	8			9		

Values represent mean ± SD. HC- k_{HbO_2}, hemolysis-corrected k_{HbO_2}; SC- k_{HbO_2}, shape-corrected k_{HbO_2}. For each comparison we use paired two-tailed t-test.

Table 4. Summary of all hematological data obtained from four strains of mice†

Mouse / Parameter	WT			AQP1-KO			RhAG-KO			dKO		
Sex	M	F	M+F	M	F	M+F	M	F	M+F	M	F	M+F
N	9	15	24	14	8	22	17	12	29	10	7	17
Age weeks	12.2 ± 2.5	13.8 ± 3.0	13.2 ± 2.9	12.1 ± 2.5	14.0 ± 2.9	12.8 ± 2.7	14.1 ± 3.0	14.4 ± 4.0	14.2 ± 3.4	12.6 ± 2.9	15.0 ± 0.6	13.6 ± 2.5
WBC $10^3/\mu l$	12.1 ± 4.7	10.2 ± 2.6	10.9 ± 3.6	12.9 ± 3.8	14.5 ± 4.1	13.5 ± 3.9	13.6 ± 4.2	10.7 ± 4.4	12.4 ± 4.4	12.0 ± 3.6	10.7 ± 2.5	11.5 ± 3.2
LYM $10^3/\mu l$	9.8 ± 3.8	8.5 ± 2.2	9.0 ± 2.9	11.0 ± 3.4	12.3 ± 3.0	11.5 ± 3.2	11.4 ± 3.6	9.0 ± 3.8	10.4 ± 3.8	10.1 ± 3.3	9.1 ± 2.4	9.7 ± 2.9
MONO $10^3/\mu l$	0.6 ± 0.2	0.4 ± 0.2	0.5 ± 0.2	0.5 ± 0.2	0.6 ± 0.2	0.5 ± 0.2	0.5 ± 0.2	0.5 ± 0.2	0.5 ± 0.2	0.5 ± 0.1	0.5 ± 0.1	0.5 ± 0.1
GRAN $10^3/\mu l$	1.7 ± 1.0	1.2 ± 0.4	1.4 ± 0.7	1.4 ± 0.6	1.6 ± 1.1	1.5 ± 0.8	1.7 ± 1.0	1.2 ± 0.6	1.5 ± 0.9	1.4 ± 0.4	1.2 ± 0.2	1.3 ± 0.4
LYM %	81.9 ± 5.3	83.8 ± 4.2	83.1 ± 4.7	84.8 ± 5.7	85.7 ± 4.2	85.1 ± 5.1	83.4 ± 7.1	83.5 ± 4.2	83.4 ± 6.0	83.8 ± 3.3	84.1 ± 3.5	83.9 ± 3.3
MONO %	4.4 ± 1.2	3.9 ± 0.6	4.1 ± 0.9	3.7 ± 1.0	3.4 ± 0.8	3.6 ± 0.9	3.8 ± 0.8	4.0 ± 0.8	3.9 ± 0.8	3.6 ± 0.8	4.2 ± 1.1	3.8 ± 0.9
GRAN %	13.7 ± 4.7	12.3 ± 3.7	12.8 ± 4.1	11.6 ± 4.8	10.9 ± 3.5	11.3 ± 4.3	12.8 ± 6.7	12.6 ± 3.5	12.7 ± 5.5	12.6 ± 2.8	11.7 ± 2.6	12.2 ± 2.7
HCT %	49.0 ± 6.1	49.0 ± 7.5	49.0 ± 6.9	48.8 ± 6.9	51.6 ± 4.3	49.8 ± 6.1	50.2 ± 7.8	50.6 ± 9.9	50.3 ± 8.6	54.4 ± 6.9	49.6 ± 4.2	52.4 ± 6.3
HGB g/dl	15.5 ± 1.2	15.5 ± 2.3	15.5 ± 1.9	15.2 ± 1.7	16.1 ± 0.5	15.5 ± 1.5	14.6 ± 2.0	14.7 ± 2.4	14.6 ± 2.1	16.0 ± 1.3	14.8 ± 0.9	15.5 ± 1.3
RDWa fl	33.0 ± 3.7	31.8 ± 2.3	32.3 ± 2.9	32.7 ± 2.3	32.4 ± 2.6	32.6 ± 2.3	35.1 ± 2.1	34.6 ± 1.9	34.9 ± 2.0*	35.3 ± 2.8	34.0 ± 1.5	34.7 ± 2.4*
RDW %	18.4 ± 1.6	17.5 ± 1.0	17.9 ± 1.3	17.6 ± 0.5	17.4 ± 0.6	17.6 ± 0.6	17.5 ± 0.6	17.2 ± 0.4	17.4 ± 0.5	18.2 ± 0.8	17.5 ± 0.6	17.9 ± 0.8
MCV fl	46.6 ± 2.8	46.6 ± 3.6	46.6 ± 3.2	47.3 ± 2.6	47.5 ± 3.6	47.3 ± 2.9	50.3 ± 1.5	50.5 ± 1.4	50.4 ± 1.5*	49.1 ± 3.4	49.4 ± 1.1	49.2 ± 2.7*
MCH pg	14.8 ± 0.9	14.7 ± 0.4	14.7 ± 0.6	14.8 ± 0.8	14.9 ± 0.4	14.8 ± 0.7	14.7 ± 0.5	14.8 ± 0.5	14.7 ± 0.5	14.5 ± 0.4	14.8 ± 0.4	14.6 ± 0.4
MCHC g/dl	31.7 ± 2.0	31.6 ± 1.9	31.7 ± 1.9	31.4 ± 3.1	31.5 ± 2.2	31.4 ± 2.7	29.2 ± 1.1	29.3 ± 1.3	29.2 ± 1.1*	29.6 ± 2.2	30.0 ± 0.9	29.8 ± 1.8*
RBC $10^6/\mu l$	10.5 ± 1.0	10.6 ± 1.6	10.5 ± 1.4	10.3 ± 1.3	10.8 ± 0.5	10.5 ± 1.1	10.0 ± 1.5	10.0 ± 1.8	10.0 ± 1.6	11.1 ± 1.0	10.0 ± 0.7	10.6 ± 1.0
PLT $10^3/\mu l$	294.1 ± 152.1	320.9 ± 180.8	310.8 ± 167.7	303.6 ± 146.6	325.9 ± 117.7	311.7 ± 134.3	377.6 ± 179.6	261.4 ± 141.1	329.6 ± 172.2	353.2 ± 158.9	255.9 ± 118.7	313.1 ± 148.1
MPV fl	6.4 ± 0.5	6.4 ± 0.7	6.4 ± 0.6	6.4 ± 0.6	6.6 ± 0.6	6.5 ± 0.6	6.6 ± 0.5	6.5 ± 0.4	6.5 ± 0.5	6.4 ± 0.6	6.3 ± 0.5	6.4 ± 0.5

†These data include only control RBCs (i.e., those not treated with drugs). Results are presented as mean ± SD. Each "N" represents an analysis of the blood from 1 mouse. We performed full hematology screens on fresh blood from WT and KO mice. We analyzed data using a one-way ANOVA, followed by the Holm-Bonferroni (Holm, 1979) correction (see Methods[107]). For each parameter (e.g., MCV), we made all possible comparisons within a row. The only 6 significant differences (indicated by *) involved RhAG-KO vs. WT or dKO vs. WT, and none were sex related. M, male; F, female; dKO, double knockout); WBC, white blood cells; LYM, lymphocytes; MONO, monocytes; GRAN, granulocytes; HCT, hematocrit; HGB, hemoglobin; RDWa, RBC average distribution width; RDW %; MCV, mean corpuscular volume; MCH, mean corpuscular hemoglobin; MCHC, mean corpuscular hemoglobin concentration; RBC, red blood cells; PLT, platelet; MPV, mean platelet volume. In paper #2[108], we summarizes a subset of the above data from mice that we used in imaging flow cytometry and mathematical simulations.

[107] See Methods>StatisticalAnalysis

[108] See Paper #2>table 4, which is a subset of the larger data set in this table.

Table 5. Summary of automated hematology data obtained from mice used in Inhibitor study†

Parameter \ Mouse	WT			dKO		
N	13			13		
Age weeks	11.9 ± 1.0			11.2 ± 0.7		
groups	Ctrl	pCMBS	DIDS	Ctrl	pCMBS	DIDS
WBC $10^3/\mu l$	3.3 ± 2.8	1.6 ± 0.6	2.2 ± 4.1	6.0 ± 4.6	2.3 ± 1.9*	3.3 ± 1.8
LYM $10^3/\mu l$	2.6 ± 2.3	1.0 ± 0.4	1.7 ± 3.5	4.6 ± 3.9	1.6 ± 1.4*	2.5 ± 1.4
MONO $10^3/\mu l$	0.2 ± 0.2	0.2 ± 0.1	0.2 ± 0.2	0.3 ± 0.2	0.2 ± 0.2	0.1 ± 0.1
GRAN $10^3/\mu l$	0.5 ± 0.4	0.4 ± 0.2	0.3 ± 0.4	1.0 ± 0.9	0.5 ± 0.4	0.6 ± 0.8
LYM %	77.0 ± 3.9	62.4 ± 6.4*	70.4 ± 8.4*	78.0 ± 11.4	65.9 ± 12.0*	77.1 ± 11.9
MONO %	4.0 ± 1.1	9.7 ± 2.1*	4.4 ± 0.7	3.9 ± 1.2	8.2 ± 2.7*	3.5 ± 1.2
GRAN %	19.0 ± 4.0	27.9 ± 5.4*	25.2 ± 8.4*	18.2 ± 11.4	25.8 ± 12.2	19.4 ± 11.2
HCT %	33.1 ± 4.5	34.9 ± 3.4	35.4 ± 3.7	37.0 ± 6.0	39.1 ± 4.5	40.0 ± 4.0
HGB g/dl	10.5 ± 1.1	11.8 ± 0.7*	11.1 ± 0.9	11.3 ± 1.8	12.5 ± 1.3	12.1 ± 1.0
RDWa fl	29.7 ± 2.3	28.7 ± 1.9	31.7 ± 2.4	32.6 ± 1.4	31.8 ± 1.5	35.2 ± 1.7*
RDW %	16.8 ± 0.7	17.6 ± 1.1*	17.3 ± 0.5	16.5 ± 0.5	17.1 ± 0.4*	16.9 ± 0.5*
MCV (fl)	46.4 ± 3.2	44.3 ± 3.0	47.5 ± 2.8	50.2 ± 0.8	48.2 ± 1.0*	51.8 ± 1.3*
MCH pg	14.8 ± 0.4	15.0 ± 0.5	15.0 ± 0.5	15.3 ± 0.2	15.4 ± 0.3	15.6 ± 0.4
MCHC g/dl	32.1 ± 2.1	34.0 ± 2.1*	31.6 ± 1.6	30.6 ± 0.4	32.0 ± 0.6*	30.2 ± 1.0
RBC $10^6/\mu l$	7.1 ± 0.8	7.9 ± 0.6*	7.4 ± 0.6	7.4 ± 1.2	8.1 ± 0.9	7.7 ± 0.7
PLT $10^3/\mu l$	91.7 ± 87.3	64.7 ± 18.3	85.9 ± 111.5	127.5 ± 113.2	68.0 ± 45.4	84.3 ± 56.0
MPV fl (N)	6.4 ± 1.2 (9)	6.1 ± 0.4 (12)	6.2 ± 0.6 (11)	6.2 ± 1.0 (13)	6.1 ± 0.5 (11)	7.7 ± 1.2* (9)

†These data on 13×2 = 26 mice are the hematology data obtained from mice used in inhibitor study. The data include samples from obtained from mice that were also used in the imaging flow-cytometry inhibitor

studies (see paper #2[109]). Because we observed no statistically significant differences between sexes in Table 4, we grouped a males and females (same gender for one pair of WT and dKO mice on that day) for this study. dKO, double knockout Results are presented as mean ± SD. Each "N" represents an analysis of the blood from 1 mouse. We analyzed data using a one-way ANOVA, followed by the Holm-Bonferroni (Holm, 1979) correction (see Methods[110]). For each parameter (e.g., MCV) from either WT or dKO, we made all possible comparisons between Ctrl, pCMBS and DIDS treatment. * denotes a significant difference compared with Ctrl for the same genotype. Samples are tested at ostensibly 50% hematocrit (See Methods).

[109] See Paper #2>table 6, which is a subset of the larger data set in this table.

[110] See Methods>Statistical Analysis

Figure Legends

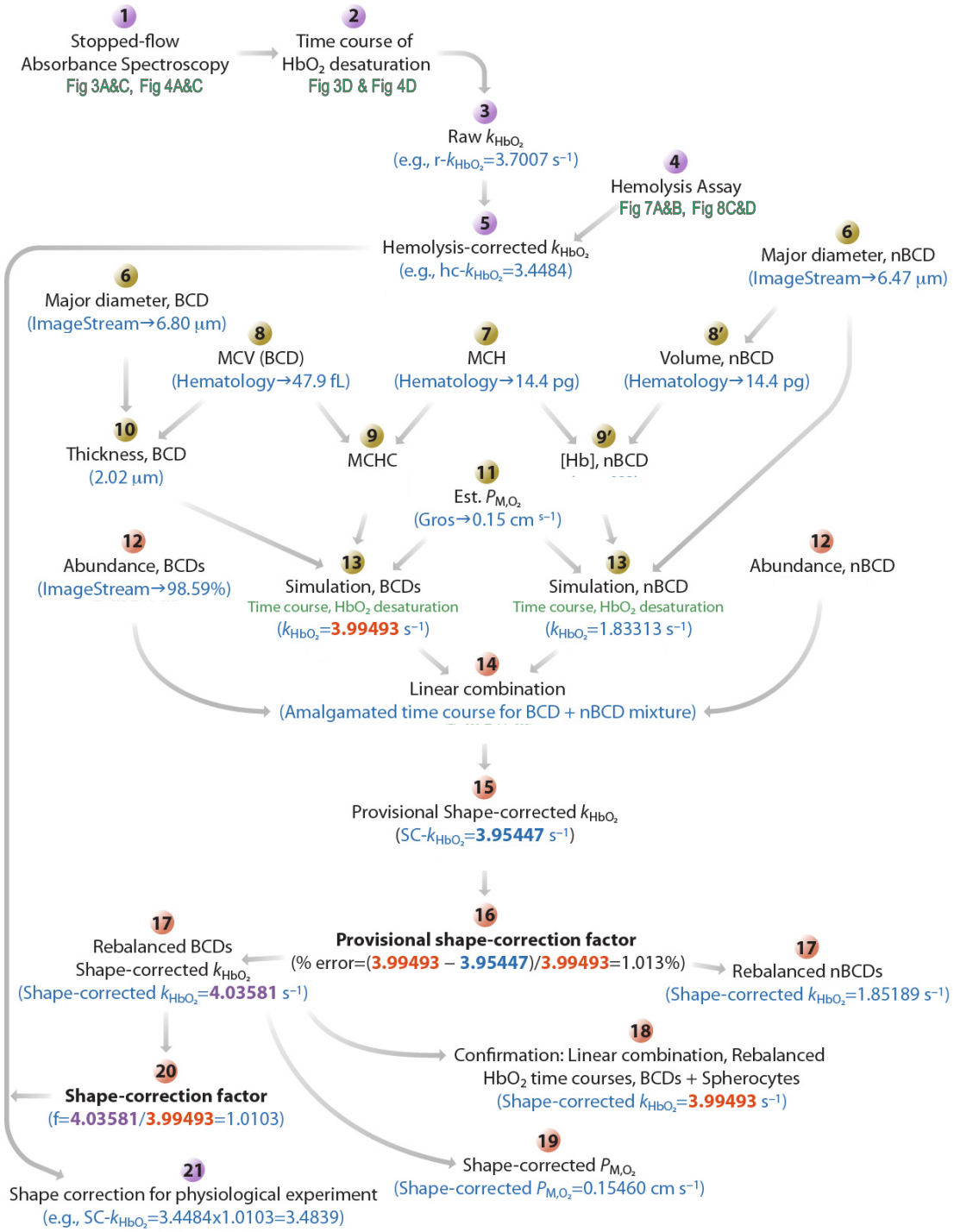

Figure 1. Workflow to obtain hemolysis-corrected and shape-corrected values of P_{M,O_2}

The numerals 1 through 21 indicate the steps summarized in the present paper—and detailed, as

appropriate, in the present paper, paper #2, or paper #3—to arrive at first a hemolysis-corrected (HC) k_{HbO2} and ultimately a shape-corrected (SC) k_{HbO_2}. At each step, we provide example values, if possible, and example figure in the present paper or papers #2 and #3.

We repeat workflow steps 1–5 for each experiment, ultimately arriving at a HC-k_{HbO2} value for each. Step 6 applies to biconcave disks (BCDs), whereas step 6' applies to non-biconcave disks (nBCDs). The same is true for steps 8 and 8', 9 and 9', 12 and 12', 13 and 13', as well as for 17 and 17'. Hb, hemoglobin; k_{HbO_2}, rate constant for deoxygenation of intracellular HbO_2; MCH, mean corpuscular hemoglobin; MCHC, mean corpuscular hemoglobin concentration; MCV, mean corpuscular volume; P_{M,O_2}; membrane permeability to O_2.

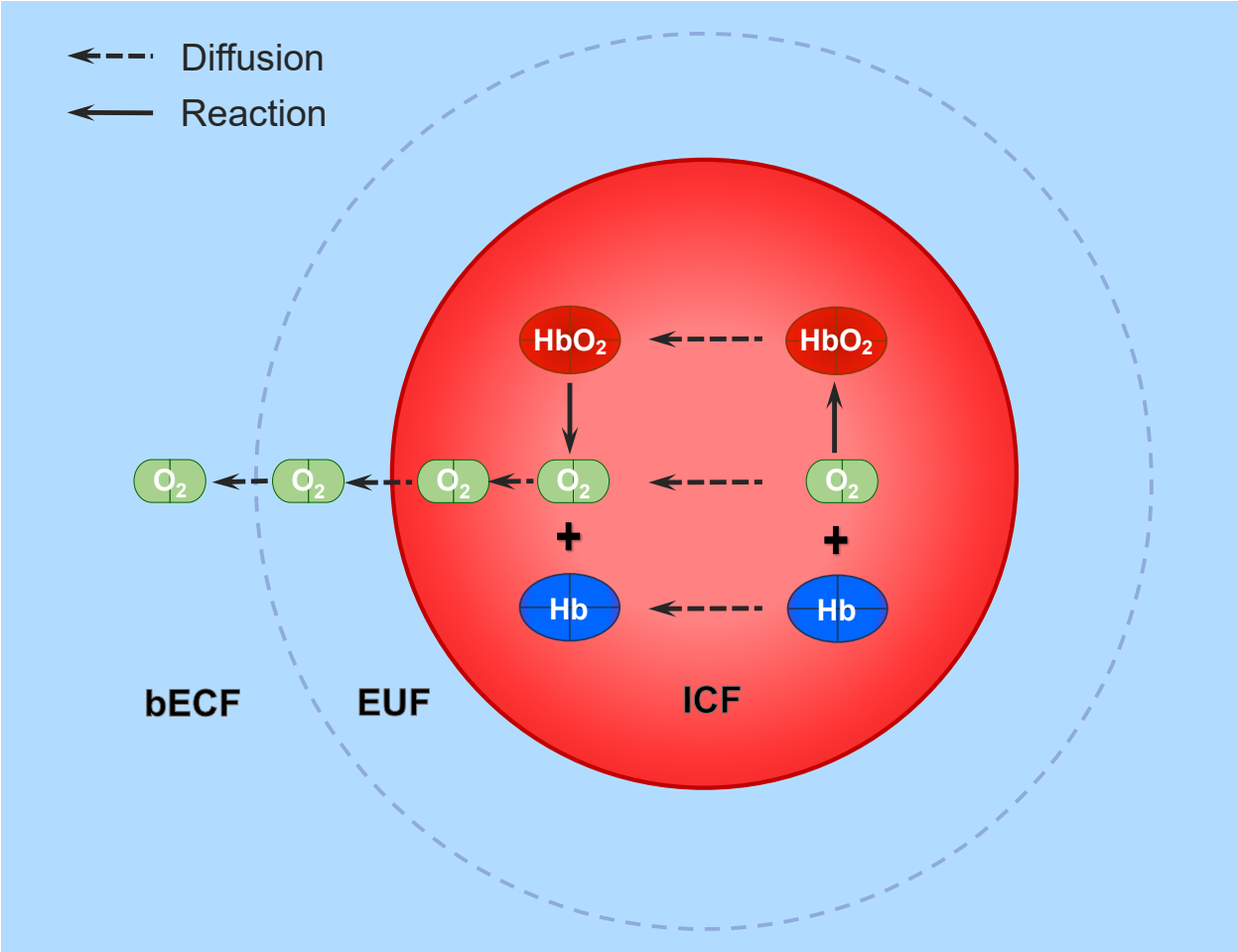

Figure 2. Model of O_2 offloading from an RBC

The model system comprises (1) plasma membrane (PM; red circle) of a spherical RBC; (2) intracellular fluid (ICF); (3) O_2, Hb, and HbO_2 within the ICF; (4) a thin layer of extracellular unconvected fluid (EUF) just external to the PM; and (5) an infinite reservoir of bulk extracellular fluid (bECF) that surrounds the EUF, as indicated by grey dashed circle. Arrows: solid black line represents reaction; dashed black line represents diffusion.

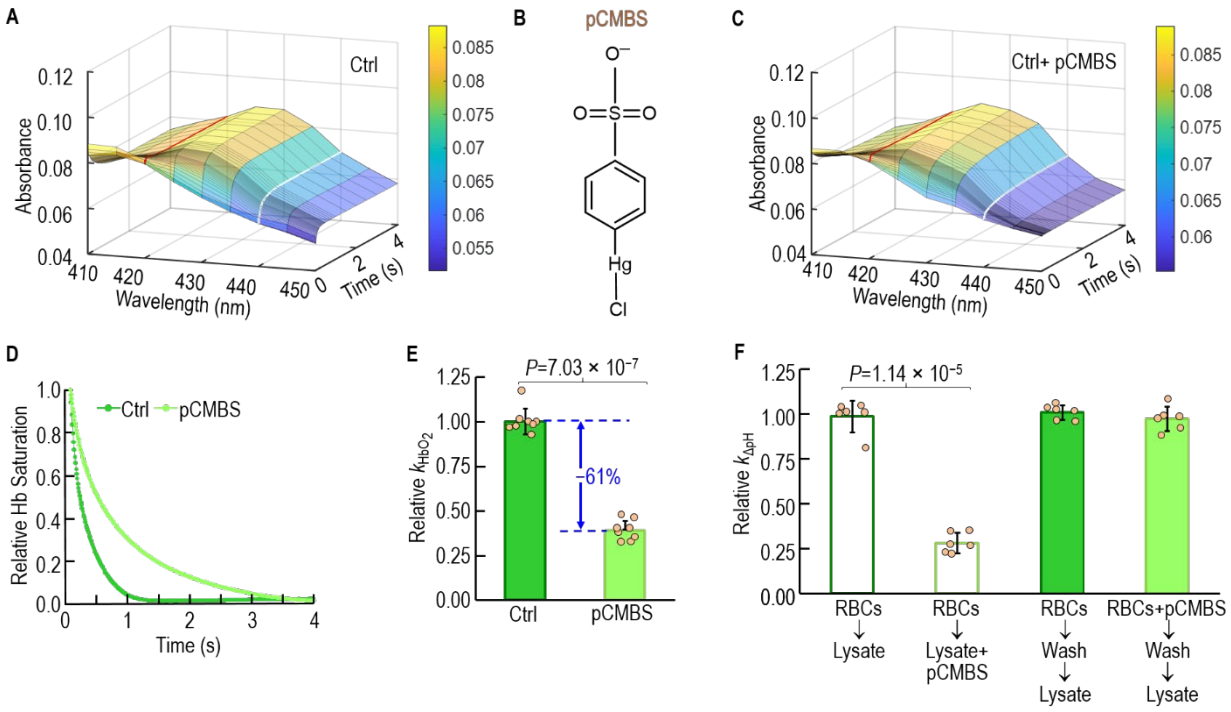

Figure 3. Effect of extracellular pCMBS on rate constant of hemoglobin deoxygenation (k_{HbO_2}) during O_2 efflux from RBCs

A, Representative time course of hemoglobin absorbance spectra during deoxygenation of ostensibly intact control wild-type (WT) RBCs. It is from a collection of spectra such as these that we compute "raw"-k_{HbO_2}.

B, Structural formula of p-chloromercuribenzenesulfonate (pCMBS).

C, Representative collection of absorbance spectra, as in panel *A*, except from WT cells treated with p-chloromercuribenzenesulfonate (pCMBS).

D, Time courses of relative hemoglobin desaturation (see Methods[111]) for the same two data sets in the previous panels.

E, Summary of effect of pCMBS on relative k_{HbO_2} in intact RBCs, corrected for both hemolysis and shape

[111] See Methods>Calculation of time course of HbO_2 desaturation>Apply weighting factors

changes, as described in Methods[112]. The absolute SC-k_{HbO_2} underlying the Ctrl bar for this data set is 3.45 $\pm$ 0.25 s^{-1}. Bars represent mean ± SD, N=8.

F, Exclusion of pCMBS from RBC cytosol. Wash solution contained 0.2% bovine serum albumin. Bars represent mean ± SD, N=6.

For *E & F,* each bar-associated point represents RBCs from 1 WT mouse. We performed paired t-tests (see Methods[113]).

---

[112] See Methods>Accommodation for hemolysis (workflow #5) >Accommodation for nBCDs (workflow #14 through #19)

[113] See Methods>Statistical analysis

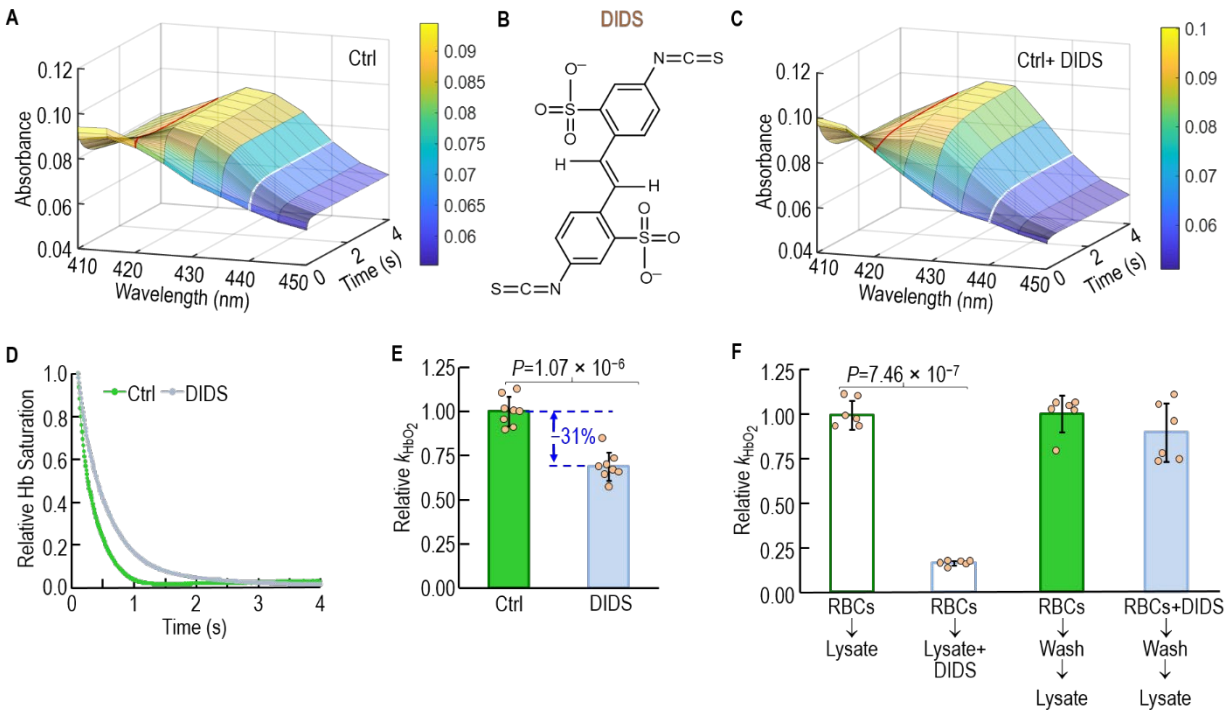

Figure 4. Effect of extracellular DIDS on rate constant of hemoglobin deoxygenation (k_{HbO_2}) during O_2 efflux from RBCs

A , Representative time courses of hemoglobin absorbance spectra during deoxygenation of ostensibly intact control wild-type RBCs. We compute "raw"-k_{HbO_2} from a collection of spectra such as these.

B, Structural formula of DIDS.

C, Representative collection of absorbance spectra, as in panel *A*, except from WT cells treated with 4,4'-diisothiocyanatostilbene-2,2'-disulfonate (DIDS).

D, Time courses of relative hemoglobin saturation (see Methods[114]) for the same two data sets in the previous panels.

E, Summary of effect of DIDS on relative k_{HbO_2} in intact RBCs, corrected for both hemolysis and shape changes, as described in Methods[115]. The absolute SC-k_{HbO2} underlying the Ctrl bar for this data set is 3.24

[114] See Methods>Calculation of time course of HbO_2 desaturation>Apply weighting factors

[115] See Methods>Accommodation for hemolysis (workflow #5) >Accommodation for nBCDs (workflow #14 through #19)

$\pm$ 0.27 s^{-1}. Bars represent mean ± SD, N=8.

F, Exclusion of DIDS from RBC cytosol. For the data underlying the two open bars, after preparing an osmotic lysate (see Methods[116]), we pretreated the hemoglobin (Hb) $\pm$ 200 μM DIDS for 60 min (1 h; see Methods[117], and determined the rate constant (k_{HbO_2}) for hemoglobin deoxygenation as described in Methods[118]. For the experiments underlying the two filled bars, the wash solution contained 0.2% bovine serum albumin. Bars represent mean ± SD, N=6.

For *E* & *F,* each bar-associated point represents RBCs from 1 WT mouse. We performed paired t-tests (see Methods[119]).

---

[116] See Methods>Preparation of RBCs>Processing of RBCs for stopped-flow studies>"osmotic lysis" in text

[117] See Methods>Preparation of RBCs>Use of inhibitors in stopped-flow studies

[118] See Methods>Calculation of "raw"-k_{HbO_2} (workflow #3)

[119] See Methods>Statistical analysis

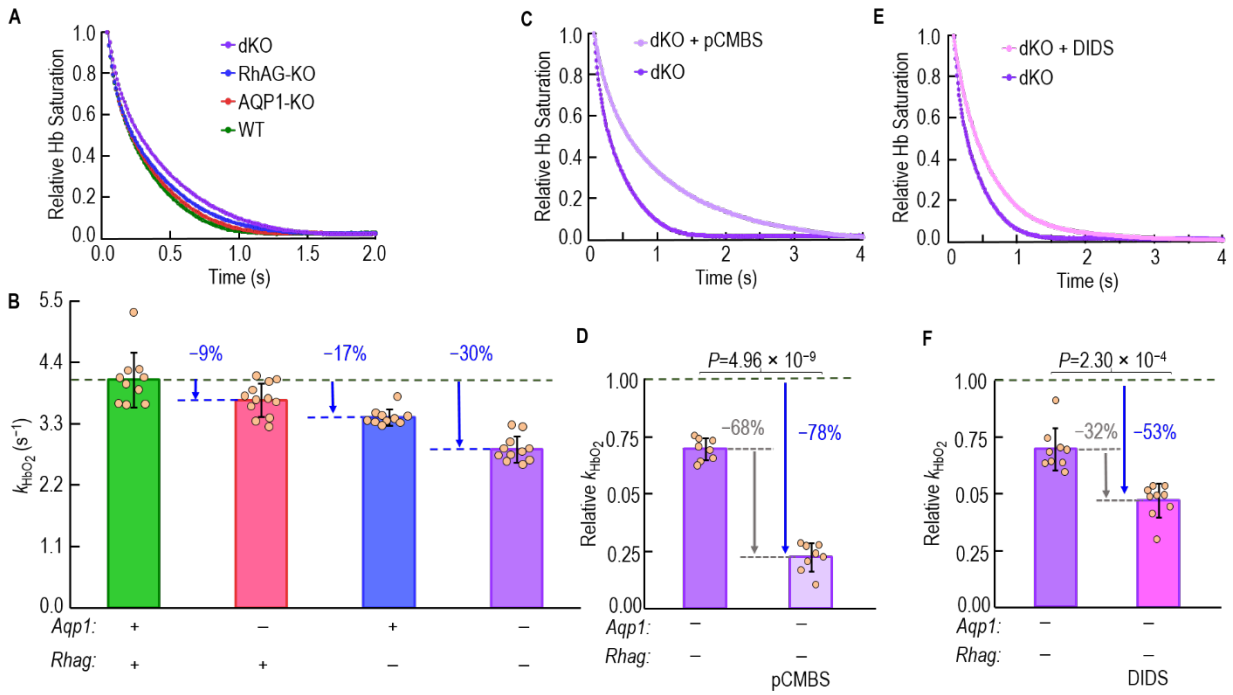

Figure 5. Effect of genetic deletions of *Aqp1*, *Rhag*, or both on rate constant of hemoglobin deoxygenation (k_{HbO_2}) during O_2 efflux from RBCs

A, Representative time courses of hemoglobin desaturation of ostensibly intact RBCs from WT mice and genetic deletions of *Aqp1*, *Rhag* or both. It is from these time courses that we compute "raw"-k_{HbO_2}.

B, Summary of mean shape-corrected k_{HbO2} (SC-k_{HbO2}) values for the full data set of which panel *A is* representative. The absolute SC-k_{HbO2} underlying the +/+ green bar for the data set in panels *B* is 4.09 ± 0.49 s^{-1} . Bars represent mean ± SD, N=10 for green bar, N=12 for red bar, N=10 for blue bar and N=11 for purple bar. Statistics for Fig 5B is for the comparison of shape-corrected k_{HbO2},(same data sets shown in Table 3B of SC-k_{HbO2}). For visual clarity we present a table of *P*-values for one-way ANOVA with Holm-Bonferroni post-hoc means comparison for the mean shape-corrected k_{HbO2} (SC-k_{HbO2}) values of all four mouse strains, as indicated in "Statistics Tables" Table 3 B3.

C & E, Representative time courses of hemoglobin desaturation of ostensibly intact RBCs, untreated or pretreated with either pCMBS (panel *C*) or DIDS (panel *E*) from dKO mice.

D & F, Summary of 2 full data sets (accommodated for hemolysis and spherocytosis) of which panels *C & E* are representative. We normalize each of the two violet bars to the height of the violet bar in *B*, and appropriately scale the pCMBS and DIDS bars. The three violet bars in panels *B, D, and F* are from three different data sets. The absolute SC-k_{HbO2} for the +/+ control RBCs (not shown here), to which we reference the two violet bars are 2.63 ± 0.18 s^{-1} for panel *D*, and 2.52 ± 0.34 s^{-1} for panel *F*. Bars represent mean ± SD. N=8 for panel *D*, N=9 for panel *F*.

For panels *B*, *D*, and *F*, each bar-associated point represents RBCs from 1 mouse, with an independent

hemolysis correction (see Methods[120]). For *B,* we performed a one-way ANOVA, followed by a Holm-Bonferroni correction (see Methods[121]). For *D & F,* we performed paired t-tests (see Methods[122]).

[120] See Methods>Accommodation for hemolysis (workflow #5)

[121] See Methods>Statistical analysis

[122] See Methods>Statistical analysis

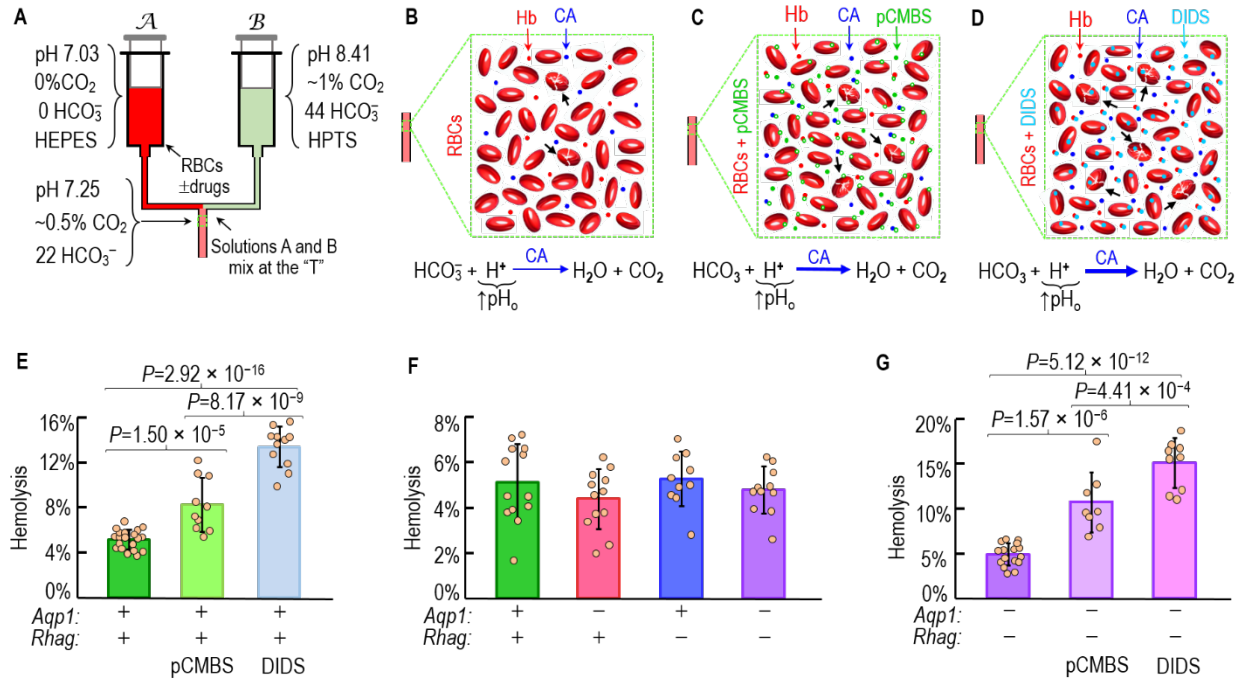

Figure 6. Degree of hemolysis in experiments on ostensibly intact RBCs

A, Schematic diagram of CO_2/HCO_3^- out-of-equilibrium (OOE) studies in stopped-flow (SF) apparatus. Solutions $\mathcal{A}$ and $\mathcal{B}$ mix at the "T" and thereby create, in the SF cell, a new solution that is out of equilibrium with ~0% CO_2/22 mM HCO_3^-/pH 7.25 at 10°C.

B, Upper panel, schematic diagram of control RBCs in an SF cell. Hemolysis is typically 0.4% as we load RBCs into the SF machine. However, in the SF reaction cell, actual hemolysis rises to ~5% for control RBCs from WT mice. The lysed cells (Black arrows) release both hemoglobin (Hb, red dots) and carbonic anhydrases (CAs, blue dots).

Lower panel, CO_2/HCO_3^- reaction. Starting from the OOE state, HCO_3^- and H^+ combine to form CO_2 and H_2O. Overall reaction is greatly accelerated by the CAs released along with Hb from the lysed RBCs. Our hemolysis assay (Zhao *et al.*, 2017) is based on the rate constant of the pH increase ($k_{\Delta pH}$) caused by this reaction.

C, Upper panel, schematic diagram of pCMBS-treated RBCs in an SF cell. Actual hemolysis in the SF reaction cell is ~8% for pCMBS-treated RBCs from WT mice. The small amount of lysis that occurs during the 15-min pCMBS pre-incubation period, before the cells enter the SF reaction cell (~0.4%), releases CA that reacts extensively with pCMBS, markedly reducing that enzymatic activity (see Figure 3*F*, open pair of bars). Later, free pCMBS enters the SF reaction cell and is exposed to a much larger amount of CA from RBCs that lyse in the SF reaction cell (~7.5%), but only for a very brief period (100's of ms). Thus, pCMBS reacts with only a tiny fraction of the newly released CA, so that extracellular CA activity is high in the SF reaction cell. The filled green dots indicate pCMBS, whereas the open green dots represent Hg that has reacted with the cell surface or with released CA.

Lower panel, CO_2/HCO_3^- reaction. Elevated extracellular CA activity from the increased hemolysis speeds

the reaction and increases $k_{\Delta pH}$, and reports the elevated hemolysis.

D, Upper panel, schematic diagram of DIDS-treated RBCs in an SF cell. Actual hemolysis in the SF reaction cell is ~13.4% for DIDS-treated RBCs from WT mice. Unlike pCMBS (panels *B*-*C*), DIDS has little effect on CA activity, so that the chemistry of the hemolysis assay is basically the same as in panel *B*. (Note that DIDS does react with Hb as shown in Figure 4*F* but HbO_2 deoxygenation is not part of our hemolysis assay). The filled light blue dots indicate DIDS, which has reacted with the cell surface and released Hb, but not released CA.

Lower panel, CO_2/HCO_3^- reaction. Because hemolysis is greater than with pCMBS in panel *C*, $k_{\Delta pH}$ is greater.

E, Summary of hemolysis in experiments on WT-mouse RBCs, either controls or cells treated with pCMBS or DIDS. RBCs were treated with 1 mM pCMBS for 15 min or 200 μM DIDS for 60 min. Bars represent mean ± SD, N=20 for green bar, N=10 for light green bar and N=11 for grey blue bar.

F, Summary of hemolysis in experiments on control mouse RBCs of all four genotypes used in the present study. Note the compressed scale of the y-axis, compared to panel *A*, which has bars for pCMBS- or DIDS-treated cells. The WT-mice RBCs represent a different data set than in panel *E*. Bars represent mean ± SD, N=13 for green bar, N=12 for red bar, N=10 for blue bar and N=11 for purple bar.

G, Summary of hemolysis in experiments on RBCs from double-knockout mice, either controls or cells treated with pCMBS or DIDS. Bars represent mean ± SD, N=17 for purple bar, N=8 for light purple bar and N=9 for pink bar.

In panels *E*, *F*, and *G*, each bar-associated point (sum of which is "N") represents 1 mouse. Bars represent mean ± SD. We performed a one-way ANOVA, followed by the Holm-Bonferroni correction (see Methods[123]).

[123] See Methods>Statistical analysis

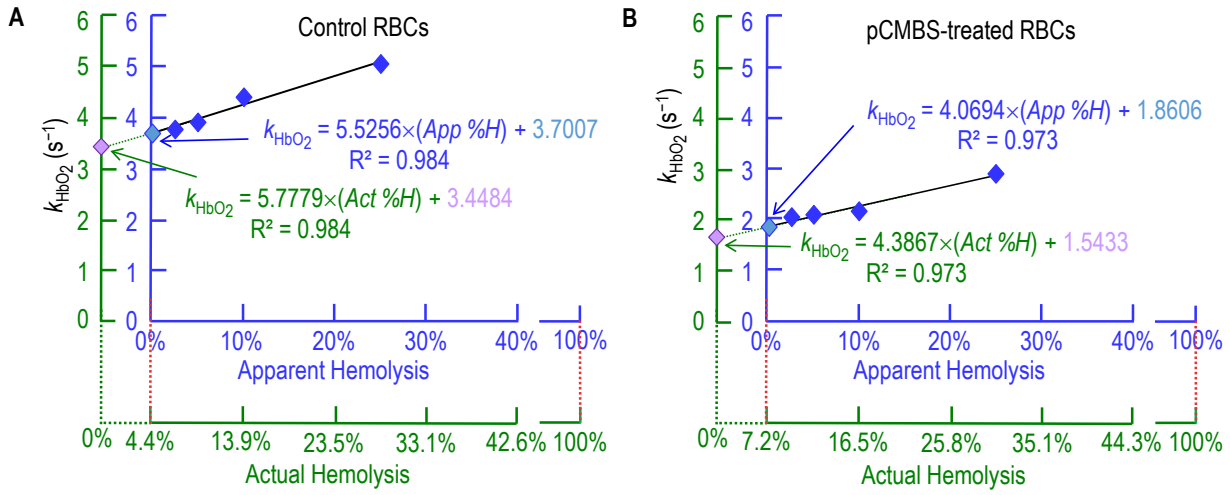

Figure 7. Accommodation of "raw"-k_{HbO_2} for hemolysis in experiments on ostensibly intact RBCs, either without inhibitors (*A*), or pretreated with pCMBS (*B*) on blood from the same WT mouse

The raw rate constant (k_{HbO_2}) is a mixture of contributions from (1) the relatively slow deoxygenation of cytosolic HbO_2 in truly intact RBCs and (2) the relatively rapid deoxygenation of extracellular HbO_2 released from hemolyzed RBCs. Here, we use a novel approach to correct "raw"-k_{HbO_2} for hemolysis in a series of 5 steps:

(1) Use the assays in Figure 6 to determine actual percent hemolysis (*Act%H*) of ostensibly 100%-intact RBCs as described in Methods[124] for control RBCs (4.4% for mouse in panel *A*) and pCMBS-treated RBCs (7.2% for mouse in panel *B*).

(2) Determine k_{HbO_2} for ostensibly 100%-intact RBCs—that is, apparent percent hemolysis [*App%H*] = 0%—as described in Methods[125]. These are the light-blue diamonds with the black perimeters in panels *A* and *B*.

(3) Determine k_{HbO_2} for mixtures of ostensibly intact RBCs (97.5%, 95%, 90%, and 75%) and fully hemolyzed RBCs (2.5%, 5%, 10%, and 25%) to keep total [Hb] = 2.5 μM in the SF reaction cell. The *App%H* values are on the blue x-axes

(4) Rescale and translate the blue *App%H* axes to obtain the green *Act%H* axes for mixtures of ostensibly

[124] See Methods> Quantitation of hemolysis in SF reaction cell (workflow #4)

[125] See Methods>Calculation of "raw"-k_{HbO_2} (workflow #3)

100%-intact RBCs and 100% hemolysate: ($Act\%H$) = ($App\%H$) + ($Act\%H_{App\%H=0\%}$)*(100% – $App\%H$).

(6) Back-extrapolate k_{HbO_2} to $Act\%H$ = 0% to obtain hemolysis-corrected k_{HbO2} values (lavender diamonds), which for the sample in panel *A* was 3.45 s^{-1} for control RBCs and, for the sample in panel *B*, 1.54 s^{-1} for pCMBS-treated RBCs. We repeat this analysis for each mouse.

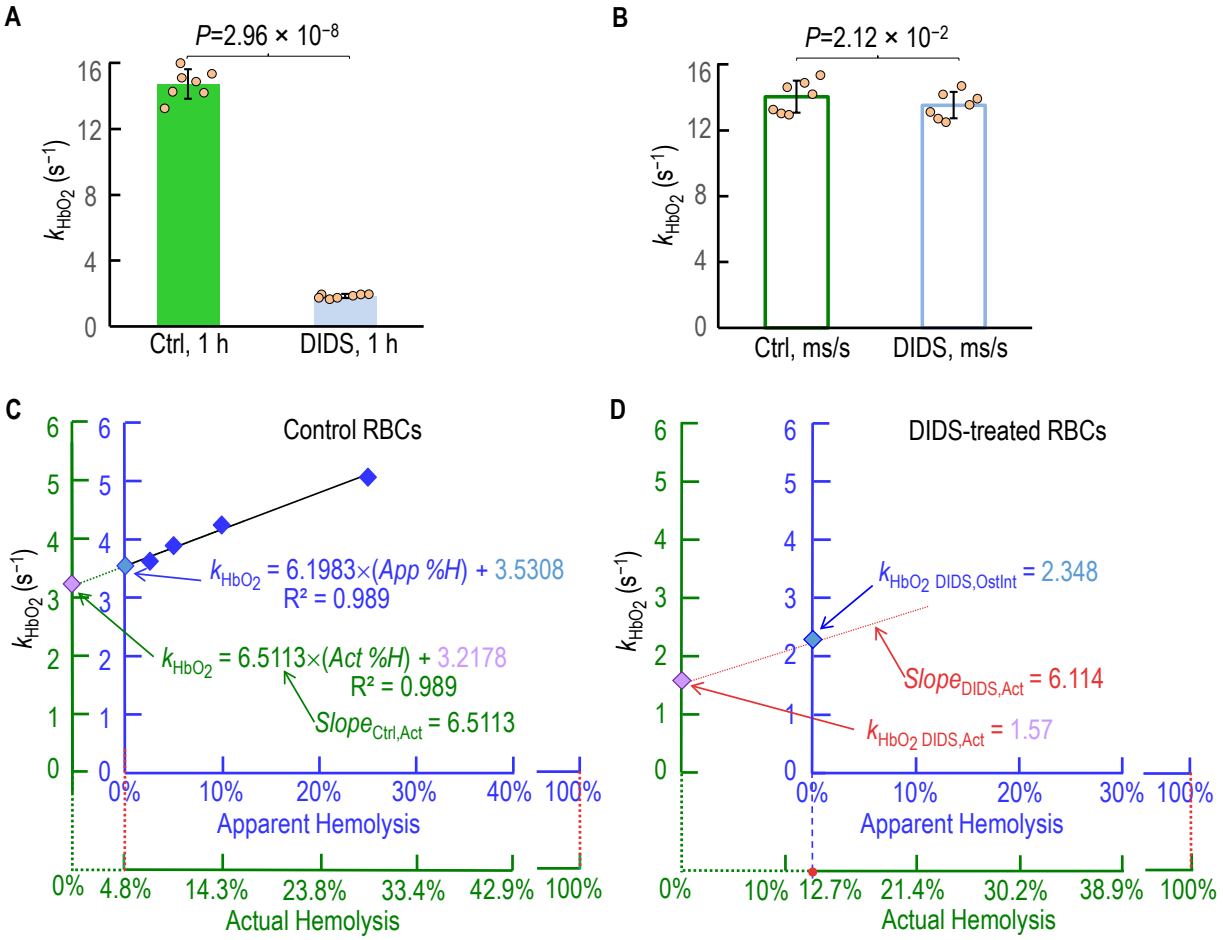

Figure 8. Correction of k_{HbO_2} for hemolysis in experiments on RBCs treated with DIDS

A, Effect of DIDS on k_{HbO_2} in a 100% hemolysate over a 1-hour time frame. This experiment is basically the same as the one summarized by the two open bars in Figure 4*E*, but on a different data set. After preparing an osmotic lysate (see Methods[126]), we pretreated the hemoglobin (Hb) ±200 μM DIDS for 60 min (1 h; see Methods[127], and determined the rate constant (k_{HbO_2}) for hemoglobin deoxygenation as described in

[126] See Methods>Preparation of RBCs>Processing of RBCs for stopped-flow studies>"osmotic lysis" in text

[127] See Methods>Preparation of RBCs>Use of inhibitors in stopped-flow studies

Methods[128].

B, Effect of DIDS on k_{HbO_2} in a 100% hemolysate over millisecond-to-second timeframe. After (1) preparing an osmotic lysate as in panel *A*, we (2) diluted the hemolysate in our oxygenated solution and the DIDS (200 μM final concentration) in our deoxygenated solution (see Table 2) as described in Methods[129], and (3) after rapid mixing of hemolysate and DIDS in the SF reaction cell, (4) determined k_{HbO2} as in panel *A*. For *A* & *B,* each bar-associated point represents RBCs from 1 WT mouse. Bars represent mean ± SD. Ctrl, control (i.e., no drugs). N=7 for each group. We performed paired t-tests as described in Methods.

C, Determination of control slope ($Slope_{Ctrl,Act}$) in plot of k_{HbO_2} vs. actual percent hemolysis (*Act%H*, green) for RBCs without inhibitors. This is the same protocol as in Figure 7*A*, though on a different data set. The Extrapolation of the k_{HbO_2} data back to *Act%H* = 0% yields an actual k_{HbO_2} (purple diamond), which in this example was 3.22 s^{-1} for control RBCs.

D, Correction of k_{HbO_2} for hemolysis in experiments on RBCs pretreated with DIDS. We determined "raw"-k_{HbO_2} values for ostensibly "100%-intact" RBCs as described for panel *C*. For the sample here in panel *D* (from same mouse as in panel *C*), this uncorrected value (blue diamond) was ~2.35 s^{-1} for DIDS-treated RBCs. We calculate the slope ($Slope_{DIDS,Act}$) of the regression line (red dashed line) using the data in panel *C*, as described in Methods[130]. Extrapolation of this line yields a hemolysis-corrected k_{HbO_2} (indicated as purple diamond for $k_{HbO_2\ DIDS,Act}$) of ~1.57 s^{-1}.

---

[128] See Methods>Calculation of "raw"-k_{HbO_2} (workflow #3)

[129] See Methods>Preparation of RBCs>Use of inhibitors in stopped-flow studies>"millisecond-to-second DIDS exposures" in text

[130] See Methods>Accommodation for hemolysis (workflow #5)>DIDS-treated RBCs

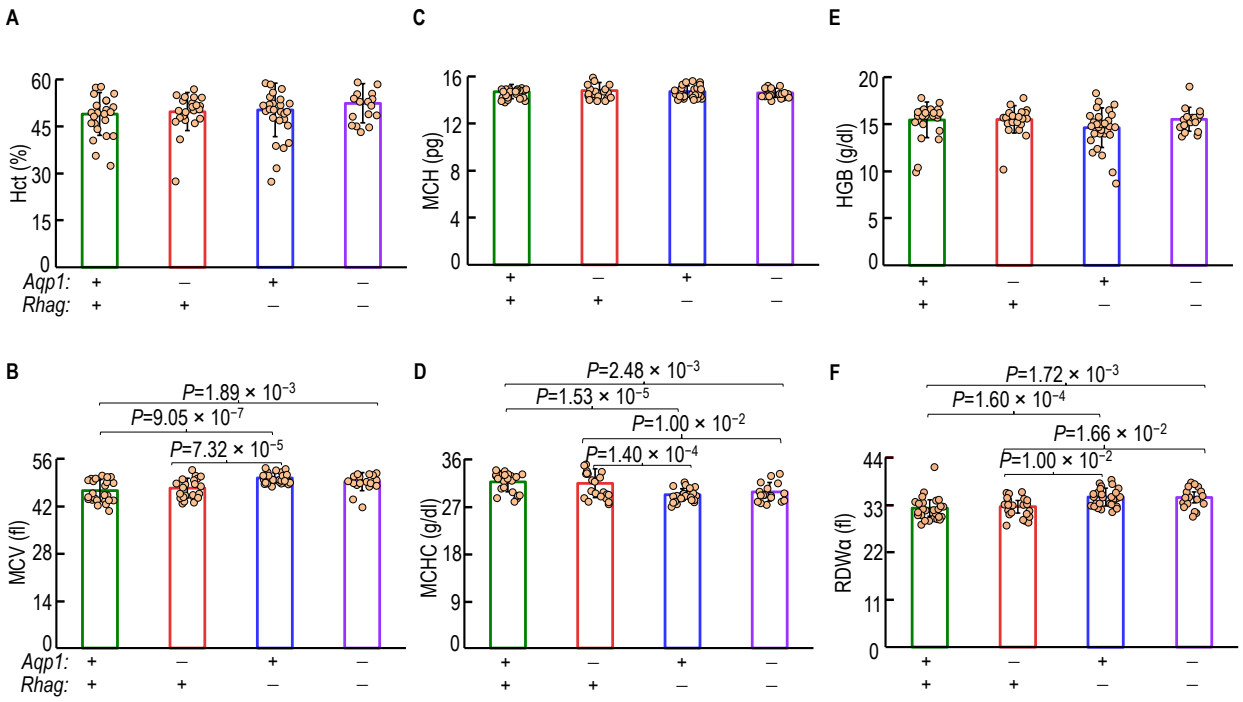

Figure 9. Effect of genetic deletions of *Aqp1*, *Rhag*, or both on key hematological parameters

The bar graphs summarize key parameter values—with data from both sexes combined—from automated hematological analyses. See Table 4 for the detailed data, separated by sexes, on WT, *Aqp1*–/–, *Rhag*–/–, and dKO mice).

A, Hematocrit (Hct).

B, Mean corpuscular volume (MCV).

C, Mean corpuscular hemoglobin content (MCH).

D, Mean corpuscular hemoglobin concentration (MCHC).

E, Hemoglobin (HGB).

F, Average of RBC distribution width (RDWa).

Each bar-associated point (sum of which is "N"added) represents RBCs from 1 mouse. Bars represent mean ± SD. N=24 for green open bar, N=22 for red open bar, N=29 for blue open bar and N=17 for purple open

bar. We performed a one-way ANOVA, followed by the Holm-Bonferroni correction (see Methods[131]).

[131] See Methods>Statistical analysis

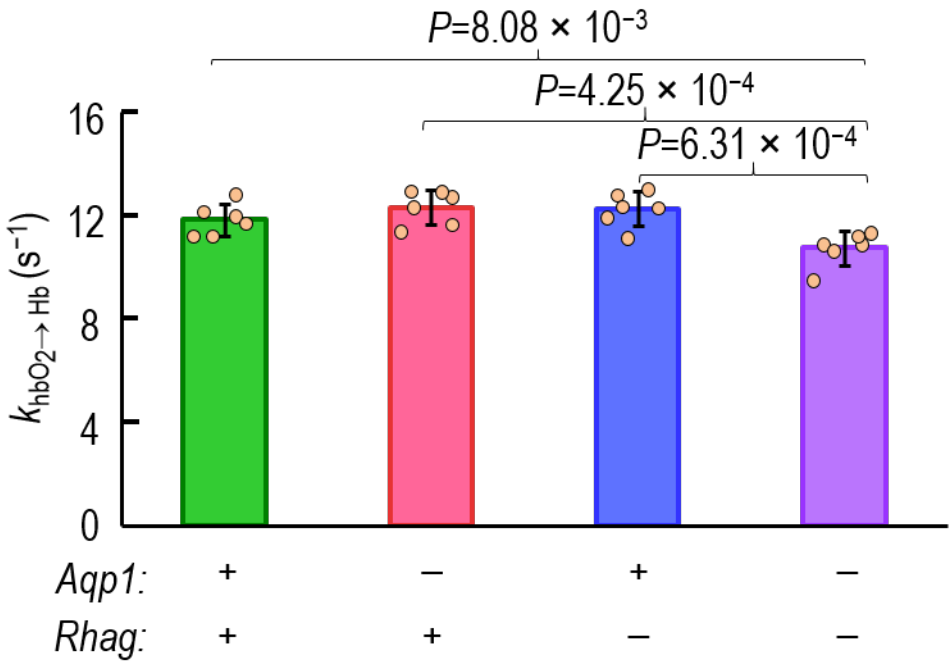

Figure 10. Effect of genetic deletions of *Aqp1*, *Rhag*, or both on rate constant of the reaction $HbO_2 \rightarrow Hb + O_2$ ($k_{HbO_2>Hb}$) in RBC lysates

See Methods[132] for a description of how we measure k_{HbO_2}. The approach here was similar, except that we worked with 100% hemolysates (see Methods[133]). Each bar-associated point represents RBCs from 1 mouse. Bars represent mean ± SD. N=6 for each bar. We performed a one-way ANOVA, followed by a Holm-Bonferroni correction (see Methods[134]).

---

[132] See Methods>Calculation of time course of HbO_2 desaturation (workflow #2) >Calculation of "raw"-k_{HbO_2} (workflow #3)

[133] See Methods>Preparation of RBCs>Processing of RBCs for stopped-flow studies>"osmotic lysis" in text

[134] See Methods>Statistical analysis

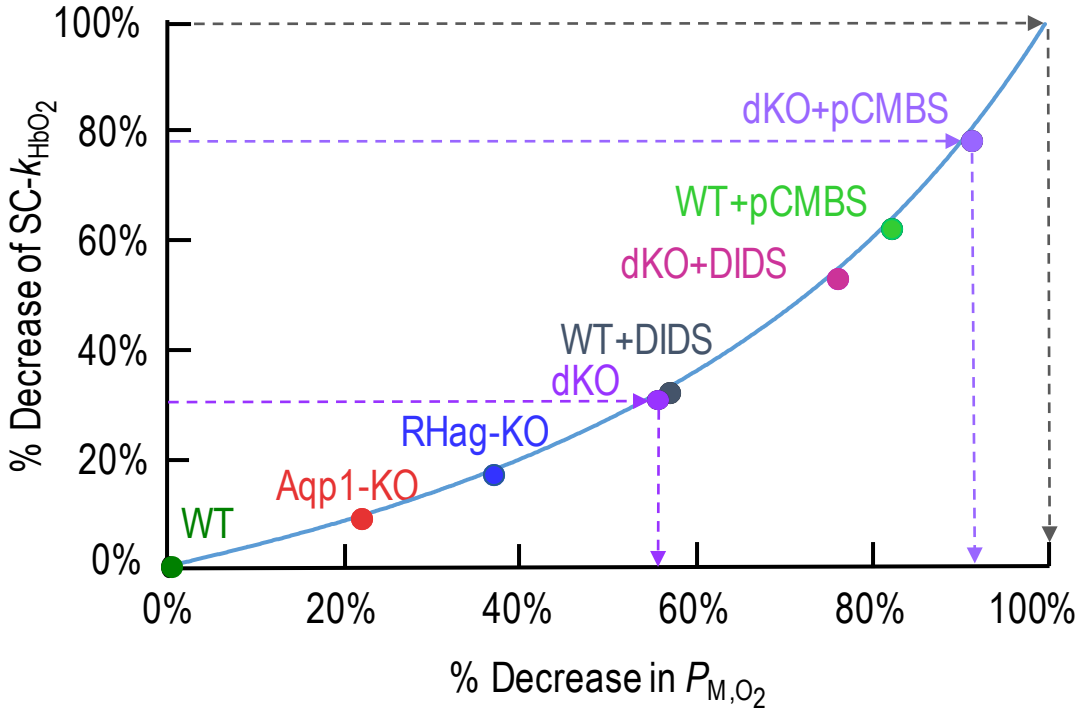

Figure 11. Dependence of percent decrease of k_{HbO_2} on percent decrease of P_{M,O_2} from macroscopic mathematical modeling and simulations

Predicted effects of decreasing the O_2 permeability of the RBC membrane (P_{M,O_2}) on k_{HbO_2}. We reference both the % decrease in k_{HbO2} (which is equivalent to the shape-corrected value of a physiological experiment) and the % decrease in P_{M,O_2} to their respective values for control (i.e., without inhibitors) wild-type (WT) cells. Note: this plot is a transformation of the modeling/simulation data in paper #3. Using our reaction-diffusion model (see paper #3[135]), we simulate the time course of HbO_2 desaturation, employing hematological and morphological data gathered for RBCs from WT mice. We then systematically decrease P_{M,O_2} (x-axis), and compute the predicted % decrease in k_{HbO_2} (y-axis; blue curve). For our 8 experimental conditions (labeled points), we used experimentally determined SC-k_{HbO_2} values to determine position on the y-axis, and then placed the points on the blue curve. Thus, the observed 78% decrease in SC-k_{HbO_2} for dKO+pCMBS (middle horizontal arrow) corresponds to a 91% decrease in P_{M,O_2} (middle downward arrow).

[135] Paper #3>Methods>Mathematical modeling and simulations

Statistics Tables

Statistics for Table 3B. For Table 3B, we use one-way ANOVA with Holm-Bonferroni post-hoc means comparison for the mean Raw k_{HbO_2} values (shown in Table 3 B1), the mean hemolysis-corrected k_{HbO_2} (HC-k_{HbO_2}) values (shown in Table 3 B2), and the mean shape-corrected k_{HbO_2} (SC-k_{HbO_2}) values (shown in Table 3 B3) of all four mouse strains. Each table is split in two halves, with FWER set at 0.05, the upper half shows the adjusted α-value for each comparison and the lower half the *P*-value. Significant *P*-values are highlighted bold.

B1, Comparison of "raw"- k_{HbO_2}

Mouse		WT	AQP1-KO	RhAG-KO	dKO
	P \ α		α	α	α
WT			0.0250	0.0167	0.000833
AQP1-KO	*P*	**0.00657**		0.0500	0.0100
RhAG-KO	*P*	**7.94×10^{-5}**	0.0912		0.0125
dKO	*P*	**3.32×10^{-10}**	**1.02×10^{-6}**	**4.52×10^{-4}**	

B2, Comparison of HC- k_{HbO_2}

Mouse		WT	AQP1-KO	RhAG-KO	dKO
	P \ α		α	α	α
WT			0.0250	0.0167	0.000833
AQP1-KO	*P*	**0.00836**		0.0500	0.0100
RhAG-KO	*P*	**1.83×10^{-5}**	**0.0258**		0.0125
dKO	*P*	**2.72×10^{-11}**	**4.59×10^{-8}**	**1.56×10^{-4}**	

B3, Comparison of SC- k_{HbO_2}

Mouse		WT	AQP1-KO	RhAG-KO	dKO
	P \ α		α	α	α
WT			0.0250	0.0167	0.000833
AQP1-KO	*P*	**5.22×10^{-5}**		0.0500	0.0100
RhAG-KO	*P*	**2.92×10^{-7}**	**0.0481**		0.0125
dKO	*P*	**1.37×10^{-15}**	**1.01×10^{-11}**	**1.21×10^{-8}**	

References

Aronson PS, Boron WF & Boulpaep E (2017). Transport of solutes and water. In *Medical Physiology: A Cellular and Molecular Approach*, 3rd Edition., ed. Boron WF & Boulpaep EL, pp. 102–141. Saunders Elsevier, Philadelphia, PA.

Ballas S, Clark M, Mohandas N, Colfer H, Caswell M, Bergren M, Perkins H & Shohet S (1984). Red cell membrane and cation deficiency in Rh null syndrome. *Blood* **63,** 1046–1055.

Blank M & Roughton FJW (1960). The permeability of monolayers to carbon dioxide. *Trans Faraday Soc* **56,** 1832–1841.

Boron WF (2010). Sharpey-Schafer lecture: gas channels. *Exp Physiol* **95,** 1107–1130.

Cabantchik ZI & Rothstein A (1974). Membrane proteins related to anion permeability of human red blood cells. I. Localization of disulfonic stilbene binding sites in proteins involved in permeation. *J Membr Biol* **15,** 207–226.

Coin JT & Olson JS (1979). The rate of oxygen uptake by human red blood cells. *J Biol Chem* **254,** 1178–1190.

Cooper GJ & Boron WF (1998). Effect of PCMBS on CO_2 permeability of *Xenopus* oocytes expressing aquaporin 1 or its C189S mutant. *Am J Physiol* **275,** C1481-1486.

Cooper GJ, Occhipinti R & Boron WF (2015). CrossTalk proposal: Physiological CO_2 exchange can depend on membrane channels. *J Physiol*; DOI: 10.1113/JP270059.

Deonikar P, Abu-Soud HM & Kavdia M (2014). Computational analysis of nitric oxide biotransport to red blood cell in the presence of free hemoglobin and NO donor. *Microvasc Res* **95,** 15–25.

Deonikar P & Kavdia M (2013). Contribution of membrane permeability and unstirred layer diffusion to nitric oxide-red blood cell interaction. *J Theor Biol* **317,** 321–330.

Endeward V (2012). The rate of the deoxygenation reaction limits myoglobin- and hemoglobin-facilitated O_2 diffusion in cells. *J Appl Physiol* **112,** 1466–1473.

Endeward V, Cartron J-P, Ripoche P & Gros G (2008). RhAG protein of the Rhesus complex is a CO_2 channel in the human red cell membrane. *FASEB J* **22,** 64–73.

Endeward V, Musa-Aziz R, Cooper GJ, Chen L-M, Pelletier MF, Virkki LV, Supuran CT, King LS, Boron WF & Gros G (2006). Evidence that aquaporin 1 is a major pathway for CO_2 transport across the human erythrocyte membrane. *FASEB J* **20,** 1974–1981.

Fick A (1855). V. On liquid diffusion. *Lond Edinb Dubl Phil Mag* **10,** 30–39.

Forster RE (1964). Rate of gas uptake by red cells. In *Handbook of Physiology*, pp. 827–837. American Physiological Society.

Geyer RR, Musa-Aziz R, Qin X & Boron WF (2013). Relative CO_2/NH_3 selectivities of mammalian aquaporins 0-9. *Am J Physiol, Cell Physiol* **304,** C985-994.

Golde WT, Gollobin P & Rodriguez LL (2005). A rapid, simple, and humane method for submandibular bleeding of mice using a lancet. *Lab Anim (NY)* **34,** 39–43.

Goossens D, Trinh-Trang-Tan M-M, Debbia M, Ripoche P, Vilela-Lamego C, Louache F, Vainchenker W, Colin Y & Cartron J-P (2010). Generation and characterisation of Rhd and Rhag null mice. *Br J Haematol* **148,** 161–172.

Graham T (1829). Notice of the singular inflation of a bladder. *Quart J Sci* **II,** 88–89.

Graham T (1833). XXVII. On the law of the diffusion of gases. *Lond Edinb Dubl Phil Mag* **2,** 175–190.

Gutknecht J, Bisson MA & Tosteson FC (1977). Diffusion of carbon dioxide through lipid bilayer membranes: effects of carbonic anhydrase, bicarbonate, and unstirred layers. *J Gen Physiol* **69,** 779–794.

Hartridge H & Roughton FJ (1927). The rate of distribution of dissolved gases between the red blood corpuscle and its fluid environment: Part I. Preliminary experiments on the rate of uptake of oxygen and carbon monoxide by sheep's corpuscles. *J Physiol (Lond)* **62,** 232–242.

Hartridge H & Roughton FJ (1928). Photographic methods of estimating the percentage saturation of haemoglobin with various gases: I. The ratio of oxyhaemoglobin to carboxyhaemoglobin. *J Physiol* **64,** 405–414.

Henry W (1803). Experiments on the quantity of gases absorbed by water, at different temperatures, and under different pressures. *Phil Trans R Soc B* **93,** 29–276.

Holland RA, Shibata H, Scheid P & Piiper J (1985). Kinetics of O_2 uptake and release by red cells in stopped-flow apparatus: effects of unstirred layer. *Respir Physiol* **59,** 71–91.

Holm S (1979). A simple sequentially rejective multiple test procedure. *Scandinavian Journal of Statistics* **6,** 65–70.

Huxley VH & Kutchai H (1981). The effect of the red cell membrane and a diffusion boundary layer on the rate of oxygen uptake by human erythrocytes. *J Physiol (Lond)* **316,** 75–83.

Kelmenson P (2016). There is no such thing as a C57BL/6 mouse! *The Jackson Laboratory*. Available at: https://www.jax.org/news-and-insights/jax-blog/2016/june/there-is-no-such-thing-as-a-b6-mouse [Accessed February 29, 2024].

Kreuzer F (1982). Oxygen supply to tissues: the Krogh model and its assumptions. *Experientia* **38,** 1415–1426.

Krogh A (1919). The number and distribution of capillaries in muscles with calculations of the oxygen pressure head necessary for supplying the tissue. *J Physiol (Lond)* **52,** 409–415.

Lauf P & Joiner C (1976). Increased potassium transport and ouabain binding in human Rhnull red blood cells. *Blood* **48,** 457–468.

Ma T, Yang B, Gillespie A, Carlson EJ, Epstein CJ & Verkman AS (1998). Severely impaired urinary concentrating ability in transgenic mice lacking aquaporin-1 water channels. *J Biol Chem* **273,** 4296–4299.

Macey RI (1984). Transport of water and urea in red blood cells. *Am J Physiol* **246,** C195-203.

Macey RI & Farmer RE (1970). Inhibition of water and solute permeability in human red cells. *Biochim Biophys Acta* **211,** 104–106.

Mathai JC, Mori S, Smith BL, Preston GM, Mohandas N, Collins M, van Zijl PC, Zeidel ML & Agre P (1996). Functional analysis of aquaporin-1 deficient red cells. The Colton-null phenotype. *J Biol Chem* **271,** 1309–1313.

Michenkova M, Taki S, Blosser MC, Hwang HJ, Kowatz T, Moss FJ, Occhipinti R, Qin X, Sen S, Shinn E, Wang D-K, Zeise B, Zhao P, Malmstadt N, Vahedi-Faridi A, Tajkhorshid E & Boron WF (2021). Carbon dioxide transport across membranes. *Interface Focus* **11,** 2.

Mitchell JK (1830). On the penetrativeness of fluids. *Am J Med Sci* **7,** 36–67.

Mitchell JK (1831*a*). On the penetrativeness of fluids. *J Roy Inst Gr Brit* **IV,** 101–118.

Mitchell JK (1831*b*). On the penetrativeness of fluids. *J Roy Inst Gr Brit* **V,** 307–321.

Mitchell JK (1833). Art. IX. On the penetration of gases. *Am J Med Sci* **13,** 100–112.

Moll W (1968). The influence of hemoglobin diffusion on oxygen uptake and release by red cells. *Respir Physiol* **6,** 1–15.

Moriyama A, Katagiri N, Nishimura S, Takahashi N & Kakeya H (2015). *In vivo* linking of membrane lipids and the anion transporter band 3 with thiourea-modified amphiphilic lipid probes. *Sci Rep* **5,** 17427.

Moss FJ, Zhao P, Salameh AI, Taki S, Wass AB, Jacobberger JW, Huffman DE, Meyerson HJ, Occhipinti R & Boron WF (2025). Role of channels in the O_2 permeability of murine red blood cells II. Morphological and proteomic studies. *bioRxiv*; DOI: https://doi.org/10.1101/2025.03.05.639962.

Musa-Aziz R, Chen L & Boron WF (2007*a*). The CO_2/NH_3 Selectivity of AQP1, AQP4, and AQP5 and How It is Affected by DIDS. *J Am Soc Nephrol* **18,** P6A.

Musa-Aziz R, Chen L-M & Boron WF (2007*b*). Differential effects of DIDS on the CO_2 vs NH_3 permeability of AQP1, AmtB, and RhAG. *Proceedings of the International Congress of Nephrology, Rio de Janeiro, Brazil*.

Musa-Aziz R, Chen L-M, Pelletier MF & Boron WF (2009). Relative CO_2/NH_3 selectivities of AQP1, AQP4, AQP5, AmtB, and RhAG. *Proc Natl Acad Sci USA* **106,** 5406–5411.

Nakhoul NL, Davis BA, Romero MF & Boron WF (1998). Effect of expressing the water channel aquaporin-1 on the CO_2 permeability of *Xenopus* oocytes. *Am J Physiol* **274,** C543-548.

Occhipinti R, Zhao P, Huffman DE, Moss FJ & Boron WF (2025). Role of channels in the O_2 permeability of murine red blood cells. III. Mathematical modeling and simulations. *bioRxiv*; DOI: https://doi.org/10.1101/2025.03.05.639964.

Overton E (1895). Über die osmotischen Eigenschaften der Zelle in ihrer Bedeutung für die Toxikologie und Pharmacologie. *Z Phys Chem* **22,** 189–209.

Overton E (1899). Ueber die allgemeinen osmotischen Eigenschaften der Zelle, ihre vermutlichen Ursachen und ihre Bedeutung für die Physiologie. *Vierteljahrsschr Naturforsch Ges Zürich* **44,** 88–135.

Parasuraman S, Raveendran R & Kesavan R (2010). Blood sample collection in small laboratory animals. *J Pharmacol Pharmacother* **1,** 87–93.

Ponder E (1948). *Hemolysis and Related Phenomena*. New York : Grune & Stratton. Available at: http://hdl.handle.net/2027/wu.89047892849.

Preston GM & Agre P (1991). Isolation of the cDNA for erythrocyte integral membrane protein of 28 kilodaltons: member of an ancient channel family. *Proc Natl Acad Sci USA* **88,** 11110–11114.

Preston GM, Carroll TP, Guggino WB & Agre P (1992). Appearance of water channels in *Xenopus* oocytes expressing red cell CHIP28 protein. *Science* **256,** 385–387.

Preston GM, Jung JS, Guggino WB & Agre P (1993). The mercury-sensitive residue at cysteine 189 in the CHIP28 water channel. *J Biol Chem* **268,** 17–20.

Rothstein A, Knauf PA, Cabantchik ZI & Balshin M (1973). The location and chemical nature of drug 'targets' within the human erythrocyte membrane. In *Drugs and Transport Processes: A Symposium*, ed. Callingham BA, pp. 53–72. Macmillan Education UK, London. Available at: https://doi.org/10.1007/978-1-349-02273-1_4.

Roughton FJW (1932). Diffusion and chemical reaction velocity as joint factors in determining the rate of uptake of oxygen and carbon monoxide by the red blood corpuscle. *Proc R Soc Lond B* **111,** 1–36.

Simon SA & Gutknecht J (1980). Solubility of carbon dioxide in lipid bilayer membranes and organic solvents. *Biochim Biophys Acta* **596,** 352–358.

Somersalo E, Occhipinti R, Boron WF & Calvetti D (2012). A reaction-diffusion model of CO_2 influx into an oocyte. *J Theor Biol* **309,** 185–203.

Stannett V (1978). The transport of gases in synthetic polymeric membranes—an historic perspective. *J Membrane Sci* **3,** 97–115.

Vallese F, Kim K, Yen LY, Johnston JD, Noble AJ, Calì T & Clarke OB (2022). Architecture of the human erythrocyte ankyrin-1 complex. *Nat Struct Mol Biol* **29,** 706–718.

Vandegriff KD & Olson JS (1984*a*). A quantitative description in three dimensions of oxygen uptake by human red blood cells. *Biophys J* **45,** 825–835.

Vandegriff KD & Olson JS (1984*b*). The kinetics of O_2 release by human red blood cells in the presence of external sodium dithionite. *J Biol Chem* **259,** 12609–12618.

Vansteveninck J, Weed RI & Rothstein A (1965). Localization of Erythrocyte Membrane Sulfhydryl Groups Essential for Glucose Transport. *Journal of General Physiology* **48,** 617–632.

Waisbren SJ, Geibel JP, Modlin IM & Boron WF (1994). Unusual permeability properties of gastric gland cells. *Nature* **368,** 332–335.

Williams JB & Kutchai H (1986). Use of a membrane-bound fluorophore to characterize diffusion boundary layers around human erythrocytes. *Biophys J* **49,** 453–458.

Wroblewski S (1879). On the nature of the absorption of gases. *Nature* **21,** 190–192.

Zhao P, Geyer RR & Boron WF (2017). A novel stopped-flow assay for quantitating carbonic-anhydrase activity and assessing red-blood-cell hemolysis. *Front Physiol* **8,** 169.

Additional Information

Data availability statement

The data that support the findings of this study are available from the corresponding authors, W.F.B., upon reasonable request.

Competing interests

The authors declare that they have no competing interests.

Author contributions

P.Z., F.J.M., R.O., R.R.G., G.G., & W.F.B. designed the study; P.Z., performed the majority of the stopped-flow experiments, and the automated hematology and analyzed the data; R.R.G., performed preliminary stopped-flow experiments; P.Z., also made the blood smears analyzed by H.J.M. P.Z., coordinated the microvideography experiments of tumbling blood cells and with D.E.H. analyzed the data; F.J.M. performed mass spectrometry and flow cytometry experiments and analyzed the data. R.O. performed the mathematical modeling and simulations and programming. D.E.H. created a program to do data analysis on raw HbSat data to produce "raw" k_{HbO_2} values. P.Z., F.J.M., R.O., & W.F.B. wrote the manuscript.